STABILITY OF A RETICULATED DOME UNDER MULTIPLE INDEPENDENT LOADS

BY

Willis S. White, III

Thesis submitted to the Graduate Faculty of the
Virginia Polytechnic Institute and State University
in partial fulfillment
of the requirements for the degree of
MASTER OF SCIENCE
in
Civil Engineering

APPROVED:

S. M. Holzer, Chairman

R. H. Plaut

G. A. Gray

March, 1978

Blacksburg, Virginia

ACKNOWLEDGEMENTS

The work presented in this thesis was carried out under the direction of , and the author wishes to express his deepest gratitude for the encouragement and guidance provided by . In addition, grateful appreciation is expressed to for reviewing the entire thesis and making valuable suggestions.

Sincere appreciation is expressed of the Writing Center of the Virginia Polytechnic Institute and State University English Department for her assistance in organizing the material and for her many constructive comments concerning the expression of ideas.

Appreciation is expressed to and for the many stimulating conversations they had with the author concerning the thesis.

The review of the thesis by and is gratefully appreciated.

The financial support provided by the Department of Civil Engineering and the computer facilities of Virginia Polytechnic Institute and State University are gratefully appreciated.

Sincere gratitude is expressed to for patiently typing the entire manuscript.

TABLE OF CONTENTS

	Page
ACKNOWLEDGEMENTS	ii
LIST OF FIGURES	v
LIST OF TABLES	vi
NOTATION	vii
I. INTRODUCTION	1
1.1 Purpose & Scope	1
1.2 Literature Review	6
a. History	6
b. Stability Boundaries	7
2. SOLUTION METHODS	11
2.1 Definitions, Principles and Theories	12
a. System Representation	12
b. Equilibrium	14
c. Stability of Equilibrium	15
d. Critical Point Classification	16
2.2 Solution Techniques	17
a. Static Perturbation	19
b. Energy Minimization	21
c. Comparison of Programs	25
d. Comparison with Published Solutions	28
3. DEMONSTRATION PROBLEMS	32
3.1 Problem Statement	32
3.2 Discussion of Results	51

Page

3.3 The Theory of Huseyin 61

4. CONCLUSIONS 63

BIBLIOGRAPHY 67

VITA 71

ABSTRACT

LIST OF FIGURES

Figure		Page
1.1	The Stability Boundary as a Design Aid	4
2.1	Equilibrium Paths	18
2.2	An Equilibrium Path Leading to a Limit Point	24
2.3	One Bar Truss Solutions - 1:1 Initial Slope	30
2.4	One Bar Truss Solutions - 1:10 Initial Slope	31
3.1	Reticulated Dome Model	33
3.2	Stability Boundary; Load Combination A ...	37
3.3	Stability Boundary; Load Combination B ...	39
3.4	Stability Boundary; Load Combination C ...	41
3.5	Stability Boundary; Load Combination D ...	43
3.6	Stability Boundary; Load Combination E ...	45
3.7	Stability Boundary; Load Combination F ...	47
3.8	Concave Stability Boundary	60

LIST OF FIGURES

Table		Page
3.1	Joint Coordinates of the Reticulated Dome in Fig. 3.1	34
3.2	Load Combinations Used to Develop Stability Boundaries	35
3.3	Points Used to Plot Fig. 3.2	38
3.4	Points Used to Plot Fig. 3.3	40
3.5	Points Used to Plot Fig. 3.4	42
3.6	Points Used to Plot Fig. 3.5	44
3.7	Points Used to Plot Fig. 3.6	46
3.8	Points Used to Plot Fig. 3.7	48
3.9	Stress Distribution	57

NOTATION

A	cross sectional area
E	Modulus of Elasticity
L	undeformed length of bar in a one bar truss
L_1	deformed length of bar in a one bar truss
O	Landau's error symbol
P	the total external load
Q	generalized displacement
Q_i	the ith generalized displacement
V	the total potential energy function
ϵ	strain
Λ	the generalized load parameter
Λ^j	the jth independent load parameter
θ	angle between bar and horizontal in a one bar truss
π	strain energy function
σ	stress
Ω	potential energy of the external forces

CHAPTER I

INTRODUCTION

1.1 Purpose & Scope

This thesis is concerned with the stability of a reticulated dome subjected to multiple independent loads. A reticulated space structure is a network of straight bar elements in which the joints lie on a curved surface [15]*. The geodesic dome invented by Fuller is one type of reticulated dome. In this thesis, a type of reticulated dome classified as a three-way grid dome [21] is studied.

Reticulated domes, because they are network structures as opposed to continuous structures, are relatively lightweight. A 130 foot reticulated dome may weigh 15 times less, but be equally as strong as the same size dome made of concrete [34]. As a result, reticulated domes have a high strength versus weight ratio and are economical from a material use standpoint. Minimal falsework and the ease of handling the individual components enables rapid erection of these structures [34]. Another advantage of reticulated domes is the uniformity of many of the components, which permits the economical use of prefabrication. In addition to their practical qualities, reticulated domes are aesthetically

---

* Numbers in brackets refer to references listed in the bibliography.

appealing, a quality noted in a variety of publications [16, 17, 21, 34].

Reticulated domes are particularly well suited for spanning large open areas. The New Orleans Superdome (680 ft span) and the Houston Astrodome (642 ft span) are two well known examples [34]; another example not so well known is the geodesic dome at the South Pole. This 52 foot high aluminum dome, spanning 264 feet, was constructed to protect enclosed buildings from wind and snow. Design live loads included a pressure load ranging from 120 psf at the apex to 300 psf at the base [29]. The individual components were all prefabricated and weigh no more than 50 lbs each [29]. Construction required less than five months total time and was performed at ground level by men wearing awkward cold weather clothing [24].

While the light weight of reticulated domes is advantageous with respect to construction and material economy, it is also the cause of a practical stability problem. With a conventional structure, the dead load is such a dominant part of the total load that variations in the live load have little effect on the stability of the structure. With a reticulated dome, however, the live load is a much more prominant part of the total load. Variations in the magnitude of localized live loads become critical because they can cause local snap-through buckling. Snap-through buckling occurs because of the small angle between the

structural elements at a joint and a plane tangent to the surface at that joint [15] and is due to the structure's poor shear load carrying capacity. Local snap-through buckling may initiate total collapse.

In 1963, a large reticulated dome in Bucharest collapsed during high winds and after fresh snow had built up in a localized concentration [2]. This failure dramatically demonstrated the significance of variations in the live load portion of the total load when the structure under consideration is a reticulated dome. Since the magnitude of live loads is rarely known exactly, the designer needs to know the stability of the structure for a range of possible live load magnitudes to ensure a safe design. This information can be obtained from stability boundaries.

The main purpose of this thesis is to develop and study stability boundaries for a shallow reticulated dome. A stability boundary outlines the mathematical region of stability in a load space and is composed of points representing critical combinations of independent loads. Stability boundaries are also referred to in the literature as load interaction curves, characteristic curves, and stability envelopes [5, 28, 34] . To select the applicable stability boundary, the designer must choose independent load configurations which can represent a possible distribution of the total load. The usefulness of the stability boundary as a design aid is portrayed in the following example.

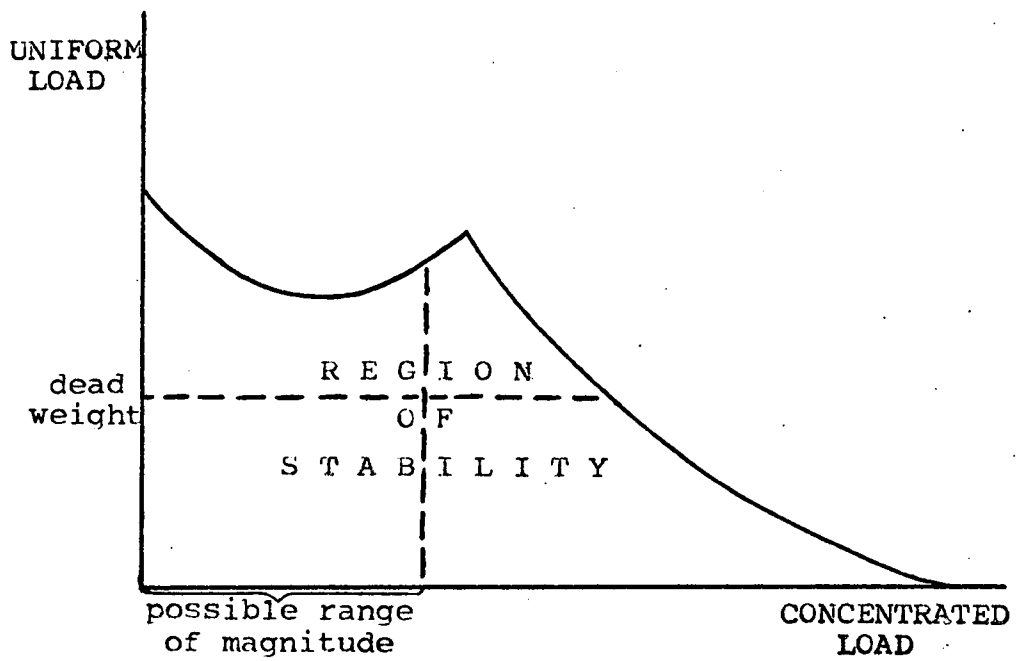

FIGURE 1.1 THE STABILITY BOUNDARY AS A DESIGN AID

Fig. 1.1 presents a stability boundary for an imaginary structure under a uniformly distributed load, such as dead weight and a concentrated load, such as a localized accumulation of snow. Using the stability boundary, the designer can easily see that the margin between the dead weight and the stability boundary, which determines the factor of safety, varies considerably over the range of possible concentrated load magnitudes. Realizing this variance, the designer can then compensate for it. Without using a stability boundary, the lower safety factors resulting from some possible load combinations might be overlooked, and result in an unsafe design.

The reticulated dome studied in this thesis has 21 degrees of freedom and a span to height ratio of approximately 12. An elastic geometrically nonlinear model is considered. Stability boundaries are plotted for several combinations of independent gravity load configurations. Symmetric and asymmetric loads are represented. The resulting stability boundaries presented consist of a curved surface displaying the interaction between three independent load configurations and 5 curves displaying the interaction between various pairs of load configurations.

To ensure the accuracy of the results two different computer programs were used to determine critical loads in this study. The program used most frequently was developed by the author from existing subroutines and

utilizes the principle of minimum potential energy. The results of this program were occasionally checked for validity by a previously developed program [1, 40] utilizing the static perturbation method. A comparison is made of the two programs and brief discussions of how they operate are presented.

The stability boundaries developed in this thesis are investigated, with emphasis placed on characterizing the points composing the boundaries and the ways that point characteristics relate to the shape of the boundaries. A method of determining lower bounds is presented. The investigation is concluded by a review of theory relevant to the particular problem studied.

1.2 Literature Review

a. History

A brief view of the development of theory dealing with stability of equilibrium will provide perspective in considering the present problem. The following short history is mainly derived from the introduction to Huseyin's recent book, Ref. 14 .

Over two centuries ago problems of elastic stability were first solved by Euler [14]. He considered the buckling of axially compressed slender columns under conservative loads and developed a linear theory for finding the critical,

or buckling, value of the load [37]. It is from this beginning that stability theory, as we now understand it, has grown. Poincaré, in a paper dealing with the stability of rotating liquid masses, was the first to systematically study the existence of branching, or bifurcation, points associated with the loss of stable equilibrium [14]. A few years later, Bryan utilized Lagrange's Theorem in developing his general theory of stability [14]. Three years after that, in 1892, Liapunov presented a mathematically rigorous general theory of stability of motion [2]. In 1930, Trefftz presented the first general formulation of the variational principle of minimum potential energy which yields the critical load [14]. Later, experiments by von Kármán and Tsien showed discrepancies between theoretical and actual shell buckling loads, indicating the possibility of nonlinear behavior [36].

In 1945, Koiter presented a systematic, nonlinear theory of stability which made possible the explanation of the failure of shells at loads below the theoretically obtained critical loads [14].

b. Stability Boundaries

The term "stability boundary" is relatively new and appears to originate with Huseyin. The concept of a stability boundary, however, predates Huseyin's work by at least thirty years; numerous examples of stability

boundaries, under different names, can be found in the literature. Timoshenko included stability boundaries for the buckling of rectangular plates under combined shear and bending stresses in a book published in 1936 [37]. Many stability boundaries have been developed to study specific problems or as design aids for certain structural forms. Some of these curves have been developed solely by experiment and some have been developed mathematically and corroborated by experiment. Numerical analysis has been used to develop curves in situations where no classical buckling formulas exist.

The following examples illustrate the variety of loads and structures for which stability boundaries have been published. Stability boundaries have been developed for cylindrical shells under torsion and external pressure [9], and under axial compression and external pressure [38]. The stability boundaries for conical shells under both of these two combinations [35, 38] and for the interaction of combined torsion and axial compression have been developed [23]. The stability boundaries for spherical shells under external pressure and a radial point load [19, 31] and for a hemisphere under external pressure and a boundary moment, and external pressure and heat [25] have also been developed. In addition, stability boundaries for various arches under self weight and a radial point load [5, 6, 7] and for arches

under three concentrated independent gravity loads [27, 39] have been developed. Stability surfaces for a skew plate under inplane stresses have been developed [20]. The idea of a curve depicting independent load interaction has even been applied to problems dealing with plastic materials [26, 32, 33]. However, with the exception of Refs. 1 and 13, there appears to be no publication in which stability boundaries are developed for a reticulated space structure.

Publications which present theory dealing with stability boundaries are quite limited at present. The earliest work appears to have been done by Papkovich[1], who presented a theorem dealing with the stability boundary of a conservative elastic system in which the total potential energy has a quadratic form. Huseyin's work extends that of Papkovich and includes theory dealing with systems in which the total potential energy is an arbitrary form. Huseyin's theorems deal with the shape of the stability boundary in the vicinity of a critical point. The work of Mandadi investigates the stability boundary at a specific type of critical point called a coincident critical point at which simultaneous (or mixed) buckling occurs [22].

The system dealt with in this paper does not have a total potential energy which is quadratic, hence it is

---

1. Papkovich published his theorem in Russian in Works on the Structural Mechanics of Ships, Vol. 4, Moscow, 1963. The theory is discussed in Refs. 14 and 28.

the more comprehensive theory of Huseyin which is of interest here. In this regard, the discussion by Roorda [30] provides a beneficial separate viewpoint. The relation of Huseyin's theory to the stability boundaries determined herein will be examined in Section 3.2.

CHAPTER 2

SOLUTION METHODS

The method used to construct the stability boundaries presented in this thesis consists of locating a number of points on the boundary and connecting these points with a curve or curves. Since the points represent critical load combinations, the accuracy of the method used to determine the critical loads is crucial. Two approaches to this problem are possible, one based on an assumption of linear pre-buckling behavior and one which takes nonlinear pre-buckling behavior into account.

Reticulated domes built today may contain hundreds of thousands of joints and members [41], making the task of performing a discrete nonlinear analysis seem enormous. The attractiveness of the assumption of linear pre-bucking behavior lies in the fact that it simplifies analysis. In a linear analysis the reticulated dome is represented by an analogous continuous dome which allows the use of classical buckling formulas [4, 34, 41]. However, classical buckling formulas only exist for load configurations which cause buckling to occur at a bifurcation point, and do not exist for problems such as a dome under gravity loads. Additionally, it has been pointed out that no rational basis exists for approximating a reticulated dome with a continuum [8, 34].

Nonlinear analysis takes advantage of numerical techniques used in conjunction with large capacity computers [3, 11, 15, 42] . The geometric nonlinearity associated with reticulated domes [1] is accounted for and response can be determined for any desired load configuration. The classification of critical points as limit or bifurcation points is made possible and critical loads can be predicted accurately for both limit and bifurcation points.

Since the majority of critical points found in this study were limit points, the accuracy available with nonlinear analysis is especially important. In the remainder of this chapter the two nonlinear analysis methods used in this study are presented.

2.1 Definitions, Principles and Theories

a. System Representation

The system under consideration can be characterized as discrete, holonomic and conservative and can be represented by its total potential energy function [13] . The potential energy is formed by adding the strain energy and the potential energy of the external forces.

$$V = \Pi + \Omega = V(Q_i, \Lambda^j) \qquad (1)$$

where

$$\Pi = \Pi(Q_i) \quad i = 1, 2, \ldots, N \qquad (2)$$

$$\Omega = \Omega(Q_i, \Lambda^j) \quad j = 1, 2, \ldots, M \qquad (3)$$

In Eqs. 1-3 Π= strain energy; Ω = the potential energy of the external forces; Q_i = the generalized displacements; N = the number of generalized displacements; Λ^j = the

generalized loading parameters; and M = the number of independent loading parameters. In this study, Ω is linear in Λ^j and can be expressed as

$$\Omega = \sum_{i=1}^{N} Q_i P_i \tag{4}$$

$$\text{where} \quad P_i = \sum_{j=1}^{M} \Lambda^j P_i{}^j \tag{5}$$

P_i is the ith generalized force component and $P_i{}^j$ is the ith component of the jth independent load configuration. An independent load configuration, P^j, is a unique constant N dimensional vector, defining the distribution of a set of forces. The individual magnitudes of these forces are determined by the value of the variable scalar Λ^j. In this study, the 21 degree of freedom structure was loaded by configurations of gravity loads at the joints. Since there were no horizontal loads, 14 components of the P^j's were consistently zero valued. For convenience, the presentation of P^j's in Chapter 3 shows only the 7 components which can assume non-zero values.

During the solution process, loading is proportional and the critical value of the total load is determined by incrementing along a load ray from the origin. Each load ray has some slope m,

$$m = \frac{\Lambda^2}{\Lambda^1} \tag{6}$$

where $0 \leq m \leq \infty$. If M = 2 in Eq. 5, then Eqs. 5 and 6

can be combined to form

$$P_i = \Lambda^1 \, (P_i^{\,1} + mP_i^{\,2}) \qquad (7)$$

Eq. 7 demonstrates that by choosing a loading ray with slope m before starting the solution process the single loading parameter Λ^1 can adequately represent the two parameter system. The stability boundary surface presented in Chapter 3 shows the interaction of 3 independent loading parameters and was constructed using several different load planes. However, it could have been constructed without using load planes by extending the loading ray concept into three dimensions. If M = 3 in Eq. 5 and

$$n = \frac{\Lambda^3}{\Lambda^1} \qquad (8)$$

where $0 \leq n \leq \infty$, then Eqs. 5, 6, and 8 can be combined to form

$$P_i = \Lambda^1 \, (P_i^{\,1} + mP_i^{\,2} + nP_i^{\,3}) \qquad (9)$$

Eq. 9 demonstrates that the single loading parameter Λ^1 can adequately represent three loading parameters as well as two and provides the basis for logical extension of the loading ray concept into systems with more than three independent parameters.

b. Equilibrium

The principle of stationary potential energy is used to form the equilibrium equations of the perturbation method, which is one of the solution techniques used. This

principle can be expressed as

$$\delta V = 0 \tag{10}$$

For an elastic system with finite degrees of freedom, such as the system under consideration, this is equivalent to [18]

$$\frac{\partial V}{\partial Q_i} = 0, \; i = 1, 2, \ldots, N \tag{11}$$

Eq. 11 forms a set of N equilibrium equations. The set of all equilibrium points in the M + N load-displacement space forms the M dimensional equilibrium surface [14].

c. Stability of Equilibrium

In this study, the stability of equilibrium is determined using the law of minimum potential energy, stated as follows:

> A conservative, holonomic system is in a configuration of stable equilibrium if, and only if, the value of the potential energy is a relative minimum [18].

To use the law of minimum potential energy, the potential energy surface in the neighborhood of an equilibrium point is examined. The change in energy about an equilibrium point can be written as [18]

$$\Delta V = \delta V + \frac{1}{2} \delta^2 V + \frac{1}{3} \delta^3 V + O(Q_i^4) \tag{12}$$

where O is Landau's error symbol. Since at an equilibrium point $\delta V = 0$, the second order term predominates. For the discrete system under consideration

$$\delta^2 V = \sum_{i=1}^{N} \sum_{j=1}^{N} \frac{\partial^2 V}{\partial Q_i \partial Q_j} \delta Q_i \, \delta Q_j \tag{13}$$

Since the system is holonomic, δQ_i, δQ_j may be arbitrary displacements. The matrix of coefficients in Eq. 13

$$\frac{\partial^2 V}{\partial Q_i \partial Q_j} \qquad i,j = 1,2, \ldots, N$$

determines the stability. If this matrix is positive definite, then ΔV in Eq. 12 will assume a positive value for any small displacement from the equilibrium state. This means that the equilibrium state in question is at a local minimum on the potential energy surface and is thus a stable state. The determinant of the matrix

$$\left| \frac{\partial^2 V}{\partial Q_i \partial Q_j} \right| \qquad i,j = 1,2, \ldots, N$$

is referred to as the stability determinant [14] and is used to determine loss of stability. Since at the origin of an equilibrium path the coefficient matrix in Eq. 13 is positive definite, the stability determinant is positive. Proceeding along the equilibrium path, a point is reached at which the stability determinant becomes zero valued. This signifies that the coefficient matrix is no longer positive definite and that we are no longer at a local minimum on the potential energy surface. Therefore, loss of stability, and the presence of a critical point, can be defined by the vanishing of the stability determinant [14].

d. Critical Point Classification

Since the above criterion for determination of critical points makes no distinction between limit points and bifur-

cation points, we must use other criteria for such classification. Two theorems presented by Thompson [36] are useful for this purpose. Fig. 2.1 illustrates Theorem 1 and Figs. 2.1b and c illustrate Theorem 2. Topological and analytical proofs for general one degree of freedom systems can be found in Ref. 36. The theorems can be stated as follows:

Theorem 1: An initially - stable (primary) equilibrium path defined by a single valued load function, the value of which increases with increasing displacement values, cannot become unstable without intersecting another distinct (secondary) equilibrium path.

Theorem 2: If an initially - stable equilibrium path which exhibits increasing load values for increasing displacement values reaches an unstable equilibrium state from which the system would exhibit a finite dynamic snap then there must be an equilibrium path exhibiting decreasing load values for increasing displacement values leaving that unstable equilibrium state. In the case of a limit point the equilibrium path leaving the unstable equilibrium state is a continuation of the original path, in the case of a bifurcation point, a second distinct equilibrium path leaves the unstable equilibrium.

Since a "finite dynamic snap" was observed at the critical load for all loads under this study, all that is needed to distinguish a bifurcation point from a limit point is to demonstrate existence of an (unstable) equilibrium path rising with the load from a critical point.

2.2 Solution Techniques

The static perturbation and energy minimization methods were used to find the necessary solutions for this investi-

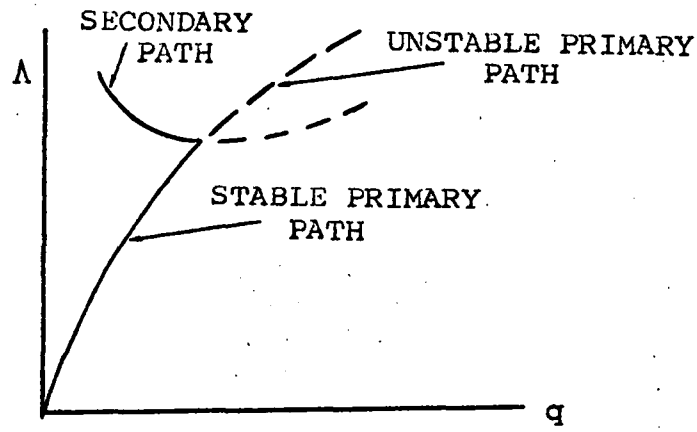

a. Intersection of Equilibrium Paths

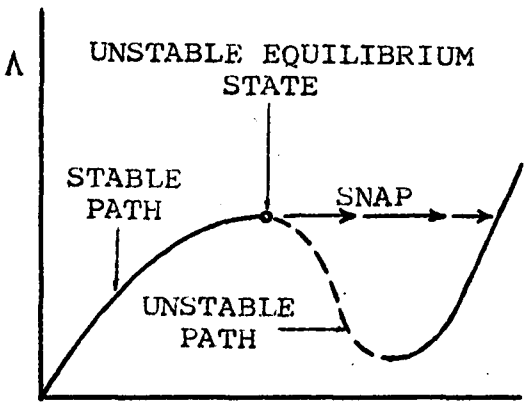

b. Limit Point

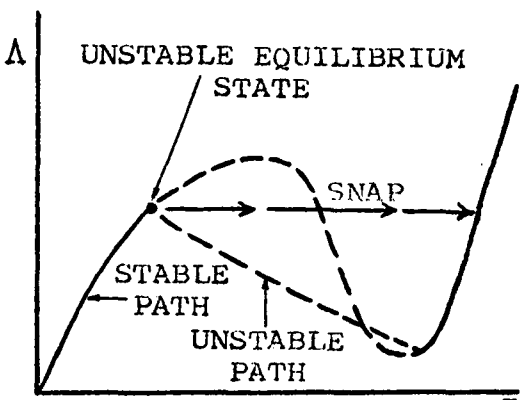

c. Bifurcation Point

FIGURE 2.1 EQUILIBRIUM PATHS

gation. However, a study of the formulation of solution techniques is not the intent of this thesis. With this in mind, the following explanations of the two methods used are presented.

a. Static Perturbation

The computer program based on the static perturbation method which is used in this study was first developed by Wongkoltoot [40] and later modified by Abatan [1, 2]. The formulation follows those presented by Huseyin, Sewell and Thompson; it differs from them mainly in that the scheme remains non-diagonalized for analysis through a bifurcation point which increases the efficiency of the solution process [1, 2]. The method has been thoroughly discussed in Ref. 2. In this section an overview of the method is presented.

Basically the static perturbation method makes use of Taylor series expansions of the nonlinear equilibrium equations about a known equilibrium state. The expansions are combined in such a way that the unknowns are expressed in terms of one variable which is designated as the perturbation parameter. There are K sets of n equations in (n + 1) unknowns formed. The number K is determined by how many terms of the Taylor series are used; n is the number of displacements. There are (n + 1) unknowns because the formulation uses one loading parameter. Since

we have (n + 1) unknowns and n equations, we specify the value of the perturbation parameter. Let m denote the order of a particular set of equations of the K sets of equations. The solution of the m ordered set of equations is required to solve the (m + 1) ordered set of equations [1] . This makes the solution to the first or lowest ordered set of equations the key solution to the remaining sets.

The technique is referred to as displacement increment or load increment depending on the variable chosen as the perturbation parameter. In this investigation, the displacement increment scheme was used because the load increment scheme was found not to be as accurate. The critical load values obtained with the load increment scheme differed from those obtained by the displacement increment scheme and the energy minimization method, which were in close agreement. One possible reason for this inaccuracy is discussed by Abatan, who argued that the choice of perturbation parameter was very important [1], and that an incorrect choice could lead to fictitious critical points. The choice of the perturbation parameter is based on an energy minimization solution for the structure in response to a small value of the load. For reasons elaborated upon by Abatan [1], the variable corresponding to the largest displacement at this value of the load is chosen as the perturbation parameter.

It can be shown [1] that the Taylor series expansion of the equilibrium equations as a function of the perturbation parameter is a power series which converges uniformly as the perturbation parameter approaches zero. Accordingly, the size of the error involved with the Taylor series approximation is dependent upon the size of the perturbation parameter; smaller values of this parameter yield smaller errors. The range of values used in this study is from 0.05 to 0.005. Additional comments concerning errors involved with the static perturbation method may be found in Ref. 1.

At a critical point the method as outlined ceases to function because the coefficient matrix of the perturbation equations becomes singular. This matrix is, in fact, the matrix discussed in section 2.1c, the determinant of which is the stability determinant. Inversion of this matrix is necessary to the solution process. The required modifications for analysis through a limit point and through a bifurcation point have been written into the program and are described in detail in Refs. 1 and 2.

b. Energy Minimization

The energy minimization method makes use of the fact that the potential energy of the structure is at a relative minimum at a stable equilibrium state. It may be thought of as a load increment, iterative procedure. Starting from a known equilibrium state a load increment is specified, which is then considered as the initial load. A predefined

energy minimization routine is used to find the equilibrium state corresponding to the minimum potential energy for the load. The load is then incremented and the energy minimization routine again minimizes the potential energy and determines a new stable configuration, this time making use of information derived with the previous solution [10]. The process continues until a discontinuity is observed in the equilibrium path, indicating a snap-through from one distinct stable equilibrium state to another. Considering that at an energy minimum the stationarity condition discussed in section 2.1b is satisfied, it follows that to minimize the potential energy is to implicitly solve the equilibrium equations for a stable equilibrium.

The minimization method used in this investigation is the Davidon-Fletcher-Powell algorithm [10], as found in subroutine DFMFP of the IBM System /360 Scientific Subroutine Package. This algorithm is an iterative modified steepest descent method [10]. For potential energy functions which are quadratic in form it has been shown to always converge [10]. Results of convergence studies for non-quadratic functions are contained in Ref. 10. The formulation contained in the DFMFP subroutine occasionally failed to converge within the allowed number of iterations, apparently caused by setting the allowable error value too small. For the problem under study, an allowable error of 10^{-8} was found to usually permit convergence within 200 iterations.

Since minimization will only determine stable equilibrium states, the critical load will not be found exactly since it occurs at an unstable equilibrium state at which snap-through takes place. The accuracy of the solution is therefore dependent on the size of the load increment. Smaller values of the load increment will result in a closer approximation to the critical load.

In order to permit critical points to be determined with more precision, the program contains a subroutine which tests for the proximity of a critical point. If the load exceeds an input test value or if the DFMFP routine fails to converge in the allowed iterations, the load increment is halved. Additionally, the slope of the equilibrium path is indirectly examined. Let m be the current equilibrium state; then (m - 1) is the previous equilibrium state and (m + 1) is the equilibrium state being computed (see Fig. 2.2). If the slope of the chord of the equilibrium path from m to (m + 1) is less than half the value of the slope of the chord from (m + 1) to m, then the load increment is halved and point (m + 1) is recomputed. This criterion is designed to detect the "flattening" of the equilibrium path that occurs in the vicinity of limit points.

It has been stated that at the critical load snap-through takes place. This was found to be true only for limit points when using the energy minimization program.

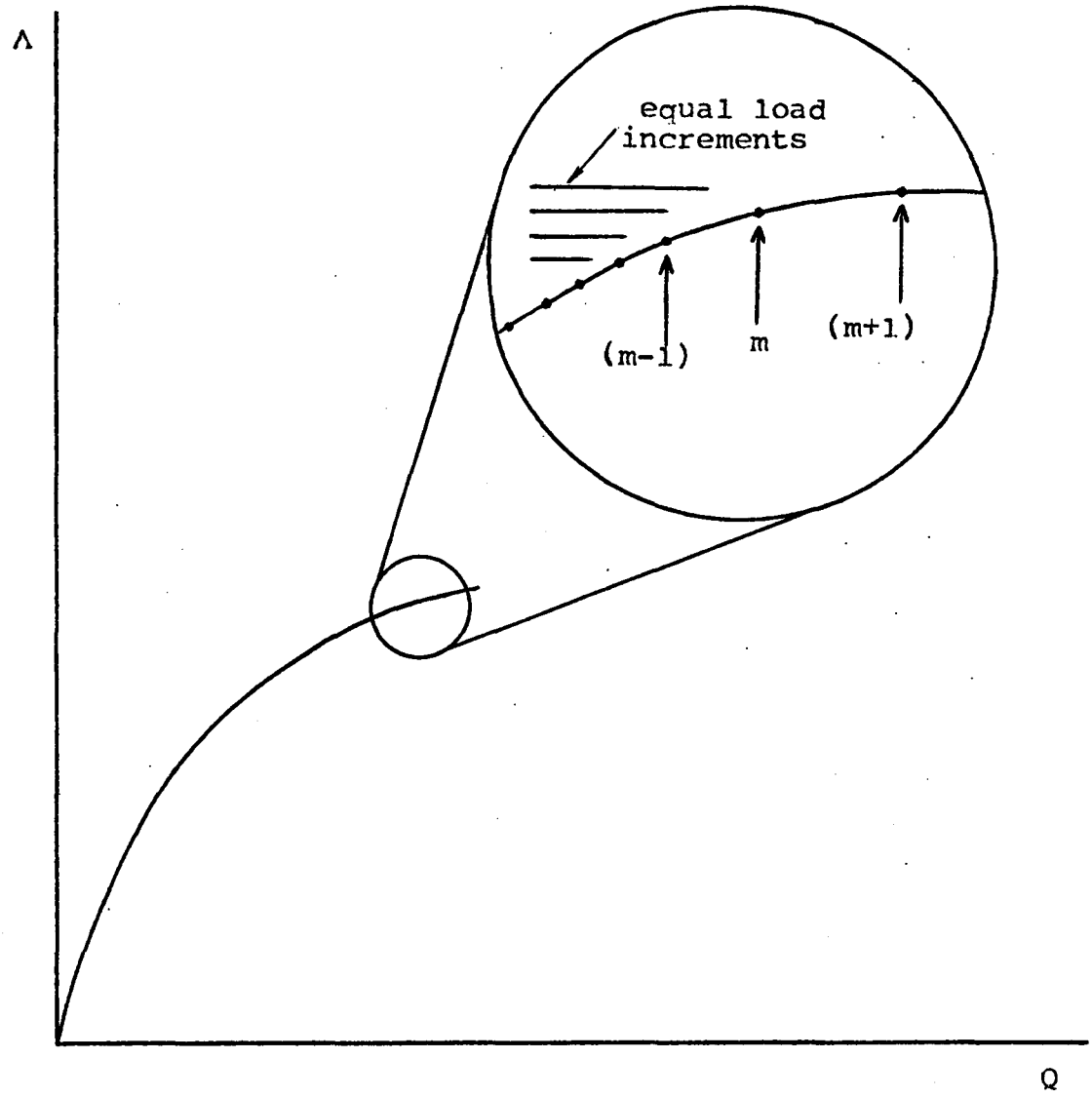

FIGURE 2.2 AN EQUILIBRIUM PATH LEADING TO A LIMIT POINT

At bifurcation points, which exhibit an unstable path along which the load increases, the program consistently converged on a small portion of what appeared to be the unstable equilibrium path before snapping through. This phenomenon was also observed by Welton [39]; currently no rigorous explanation for it exists. The existence of this peculiarity is of interest, since if this unstable portion is a true unstable equilibrium path, there would be no need to use the perturbation method to classify critical points (see section 2.1d).

c. Comparison of Programs

The static perturbation method has one great advantage over the energy minimization method; it can provide post-buckling information necessary for classifying critical points as limit or bifurcation points. However, a major concern of this study is the accurate computation of the critical load. The following comments are based on a comparison of 8 separate problems solved by both programs. Both programs use the same potential energy formulation and the same method of finding the stability determinant. Additionally, the exact strain-displacement relation is used by both programs, allowing for large displacements and large rotations [13].

The critical loads computed by the static perturbation program differ from those computed by the energy minimi-

zation program by 0.3 to 7.2 percent, with a tendency for greater difference at higher critical load values. The static perturbation program was clearly more efficient, taking less time and using less memory space to compute the same information. However, the perturbation program was also less reliable. The behavior of the program when passing through apparent bifurcation points was inconsistent; in most cases it became numerically unstable. Slight discontinuities in the immediate post critical equilibrium path were occasionally observed when numerical instability was not a problem. In contrast, the energy minimization program consistently passed through the apparent bifurcation point and converged on a small section of the apparent unstable equilibrium path with load increasing before snap-through to the stable failure configuration. The observed increase in load prior to snap through ranged from 5 to 13 percent of the critical load. This consistent behavior led to the hypothesis that the energy minimization program solutions alone might be used to classify critical points.

The gradients of the potential energy (partial derivatives of the energy with respect to displacements) represent force imbalances and provide a convenient means to judge the accuracy of the solution. At an equilibrium state the gradients should vanish. The gradients

computed by the static perturbation program tended to be of order 10^{-7}, while those computed by the energy minimization program tended to be of order 10^{-10}.

The difficulty of verifying bifurcation points with the static perturbation program, which arose because of the inconsistent post critical convergence characteristic, was overcome by using estimates of an unstable equilibrium state at a load greater than the bifurcation load. Two problems in which the perturbation program had converged on a post critical equilibrium path with decreasing load values were made to converge on such estimated unstable equilibrium states and generate unstable equilibrium paths with increasing load values, thus verifying bifurcation. The estimated unstable states were obtained from energy minimization solutions for the same problems. The perturbation program would not have converged on the estimated states if they had been inaccurate, which implies that the unstable post buckling paths somehow found by the energy minimization program were actual paths. These two cases support the unproven hypothesis that the energy minimization program solutions alone can be used as a basis for classification of critical points as limit or bifurcation points.

As a final comparison, it should be made clear that the coding of the static perturbation method calls for a much greater amount of problem information than the energy

minimization method. The energy minimization method requires the calculation of the potential energy and its first and second partial derivatives with respect to displacement. The perturbation method as used, which is a third order approximation, calls for calculation of the potential energy and its first, second, third and fourth partial derivatives with respect to displacement and load.

d. Comparison with Published Solutions

As a validation of the two programs used, solutions were compared with other published solutions. Fig. 2.3 shows the solutions to a one bar truss problem in which the initial slope of the bar is equal to unity. The closed form solution for this problem, computed by Yamada [15], is also shown. The differences are to be expected; the definition of axial strain used in Yamada's solution is

$$\epsilon = u_x + \frac{1}{2} (u_x^2 + v_x^2 + w_x^2) \qquad (14)$$

where u, v and w are the displacements along the local X, Y, and Z axes and the subscripts represent differentiation with respect to x. In this study the volumetric strain term

$$\frac{1}{2} (u_x^2 + v_x^2 + w_x^2)$$

was not included in the formulation of the solution process. This omission is felt to be justified because the size of the axial displacements in the bar buckling problem found in a reticulated dome is such that volumetric strain does

not play a significant part. This statement is verified by Fig. 2.4, which shows the energy minimization program solution vs. the closed form solution for the problem in which the initial slope of the bar is 1/10. This latter problem is more closely related to the bar buckling situation found in the structure considered by this study.

Further favorable solution comparisons are made in Ref. 13 which presents comparisons with solutions published by Hangai and Kawamata [11] and by Jagannathan, et al. [15].

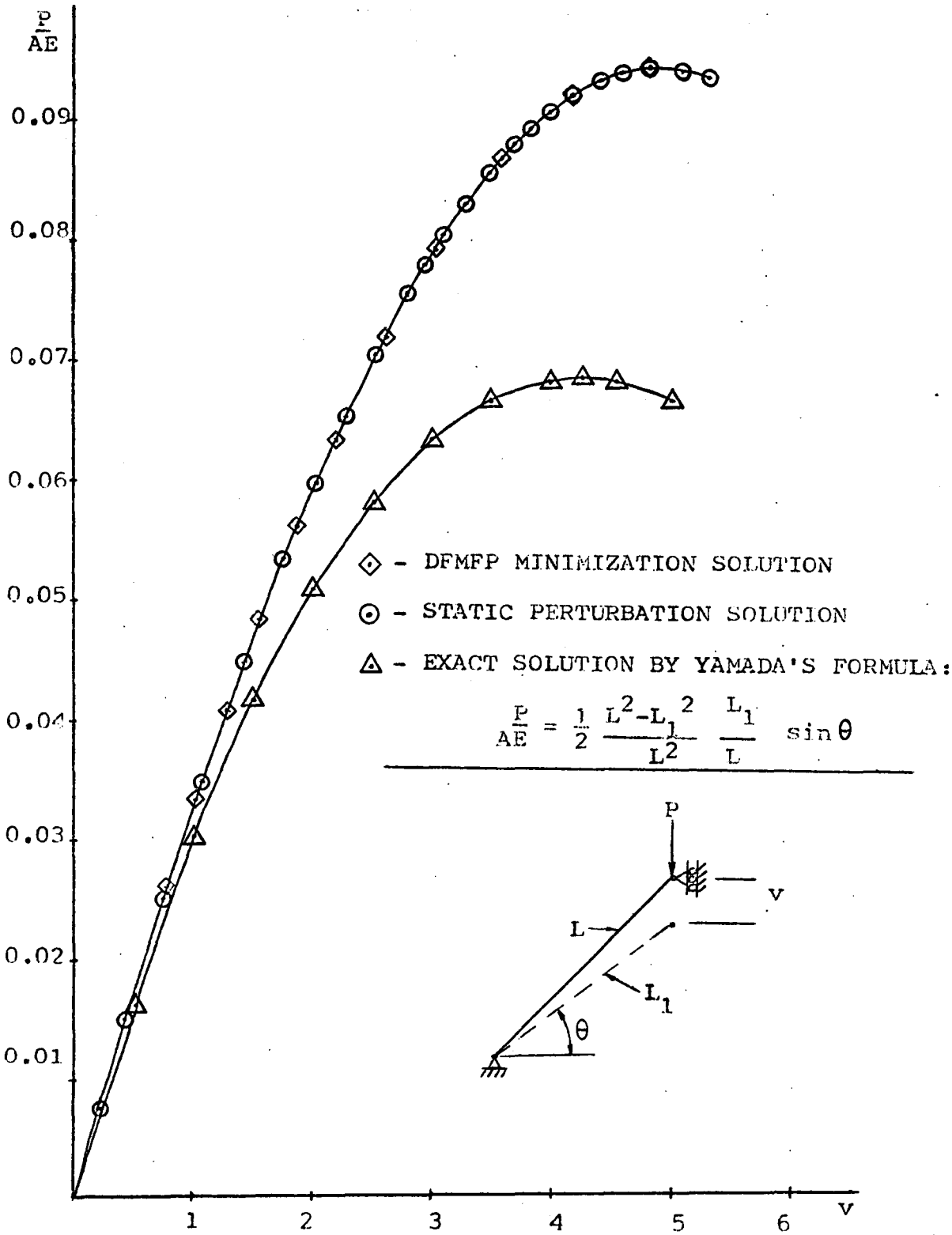

FIGURE 2.3 ONE BAR TRUSS SOLUTIONS - 1:1 INITIAL SLOPE

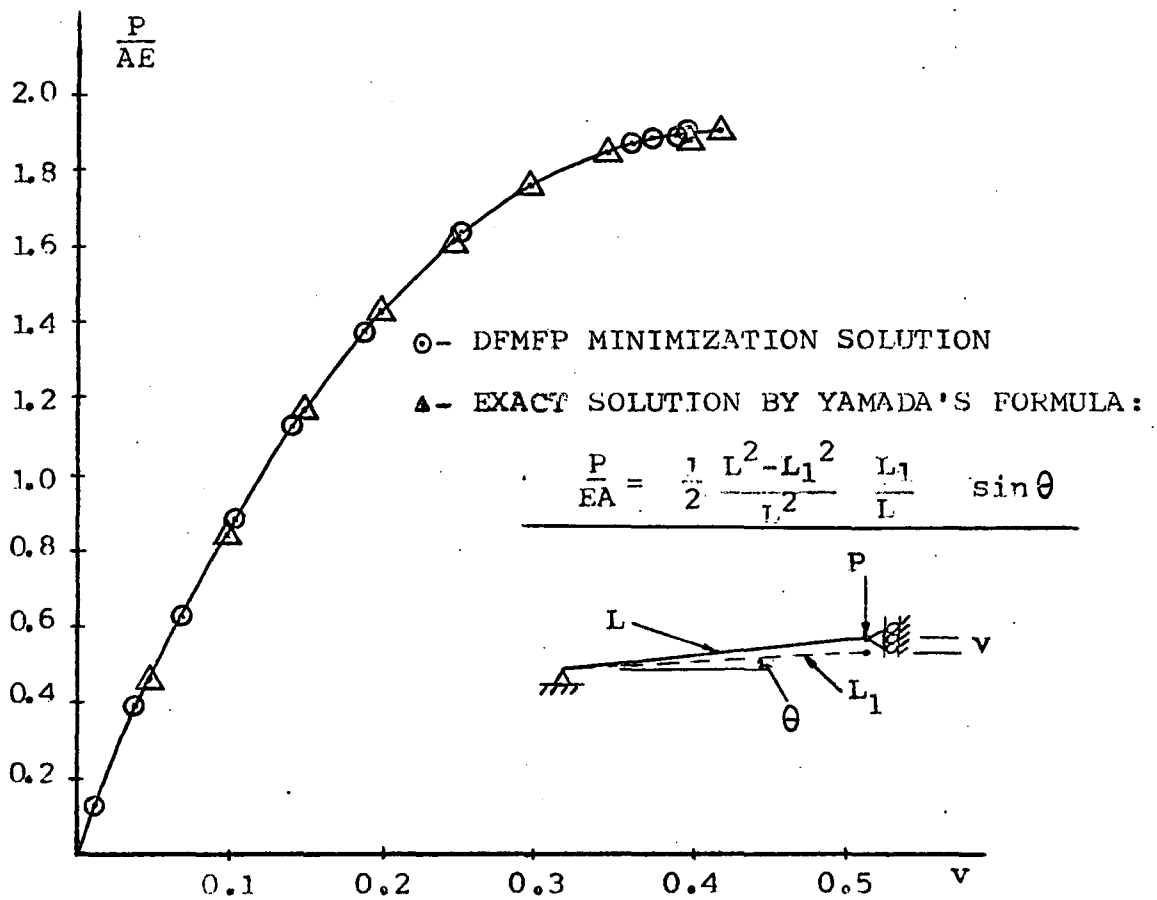

FIGURE 2.3 ONE BAR TRUSS SOLUTIONS - 1:10 INITIAL SLOPE

CHAPTER 3

DEMONSTRATION PROBLEMS

3.1 Problem Statement

The reticulated dome model of this study was previously investigated by Wongkoltoot [40], Abatan [1] and Holzer, et al. [13] . In this chapter, stability boundaries for the model are developed and presented. The points used to construct the boundaries are classified as limit or bifurcation points and buckled states corresponding to these points are noted. The use of the boundaries as design aids is discussed. A hypothesis supporting classification of critical points at cusps in the boundaries as bifurcation points is presented. An explanation for the occurrence of load maxima at cusps is offered. A method of determining lower bounds is reviewed and a theorem presented by Huseyin which concerns the convexity of the boundaries is briefly discussed.

Fig. 3.1 depicts the geometry of the model and Table 3.1 lists the joint coordinates. The choice of units of length and force is optional and determines the units of area and modulus of elasticity. All members are assumed to be prismatic and have identical cross sectional properties. Only the axial forces in the members are considered; the joints are assumed to transmit no bending moments or torques and to function as ball and socket joints. This structure might be put to practical use as the framework for a skylight, a small span roof, or a tank cover.

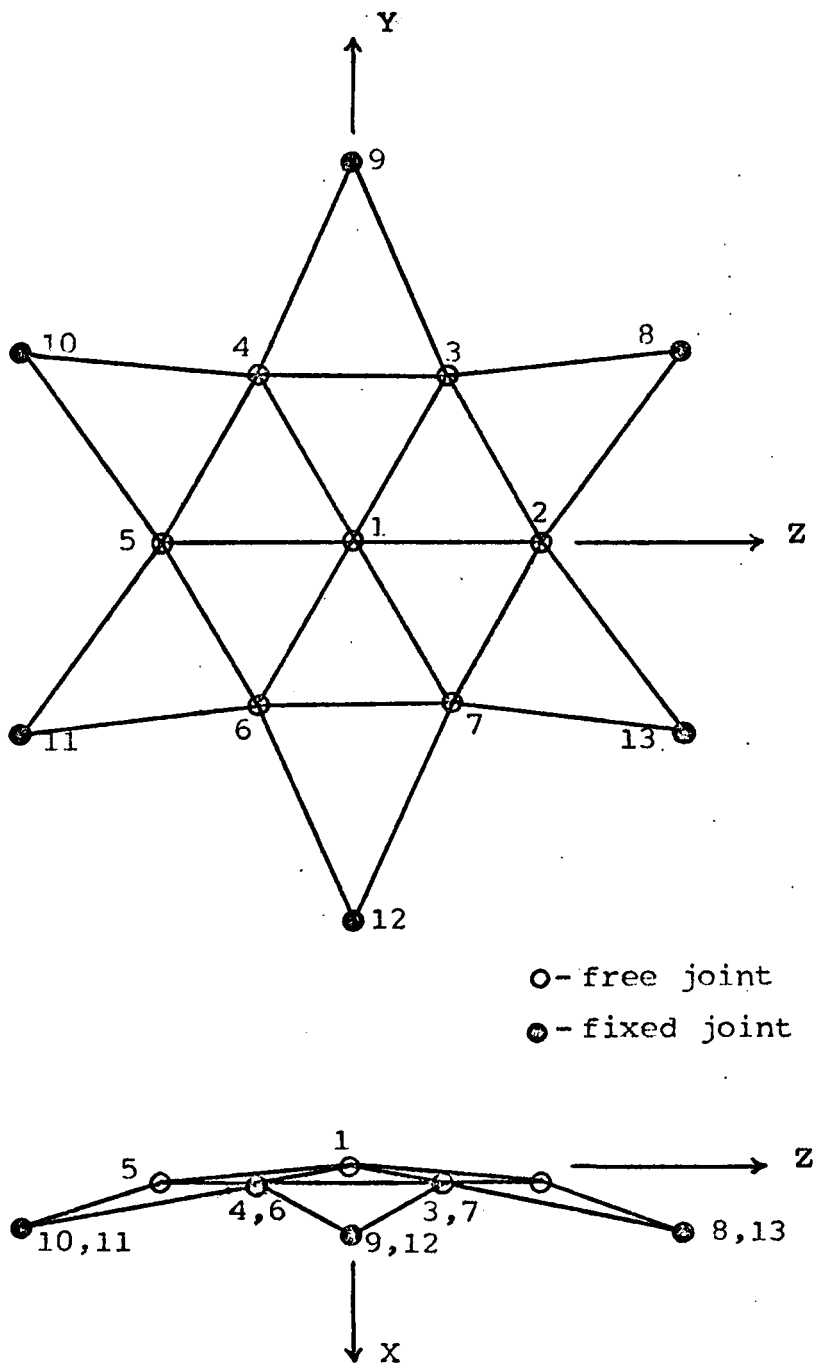

FIGURE 3.1 RETICULATED DOME MODEL

TABLE 3.1

JOINT COORDINATES OF THE RETICULATED DOME

JOINT	COORDINATES		
	X	Y	Z
1	0.0000	0.0000	0.0000
2	2.0000	0.0000	25.0000
3	2.0000	21.6500	12.5000
4	2.0000	21.6500	-12.5000
5	2.0000	0.0000	-25.0000
6	2.0000	-21.6500	-12.5000
7	2.0000	-21.6500	12.5000
8	8.1609	25.0000	43.3000
9	8.1609	50.0000	0.0000
10	8.1609	25.0000	-43.3000
11	8.1609	-25.0000	-43.3000
12	8.1609	-50.0000	0.0000
13	8.1609	-25.0000	43.3000

TABLE 3.2

LOAD COMBINATIONS USED TO DEVELOP THE STABILITY BOUNDARIES

FIGURE	LOAD COMBINATION	COMBINED INDEPENDENT LOAD CONFIGURATIONS
3.2	A	$P = \Lambda^1 \begin{bmatrix} 1 \\ 0 \\ 0 \\ 0 \\ 0 \\ 0 \\ 0 \end{bmatrix} + \Lambda^2 \begin{bmatrix} 0 \\ 1 \\ 1 \\ 1 \\ 0 \\ 0 \\ 0 \end{bmatrix}$
3.3	B	$P = \Lambda^1 \begin{bmatrix} 0 \\ 1 \\ 1 \\ 1 \\ 0 \\ 0 \\ 0 \end{bmatrix} + \Lambda^2 \begin{bmatrix} 0 \\ 0 \\ 0 \\ 0 \\ 1 \\ 1 \\ 1 \end{bmatrix}$
3.4	C	$P = \Lambda^1 \begin{bmatrix} 1 \\ 0 \\ 0 \\ 0 \\ 0 \\ 0 \\ 0 \end{bmatrix} + \Lambda^2 \begin{bmatrix} 0 \\ 1 \\ 1 \\ 1 \\ 1 \\ 1 \\ 1 \end{bmatrix}$
3.5	D	$P = \Lambda^1 \begin{bmatrix} 1 \\ 1 \\ 1 \\ 1 \\ 1 \\ 1 \\ 1 \end{bmatrix} + \Lambda^2 \begin{bmatrix} 0 \\ 1 \\ 1 \\ 1 \\ 0 \\ 0 \\ 0 \end{bmatrix}$
3.6	E	$P = \Lambda^1 \begin{bmatrix} 1 \\ 0 \\ 0 \\ 0 \\ 0 \\ 0 \\ 0 \end{bmatrix} + \Lambda^2 \begin{bmatrix} 1 \\ 1 \\ 1 \\ 1 \\ 1 \\ 1 \\ 1 \end{bmatrix}$
3.7	F	$P = \Lambda^1 \begin{bmatrix} 1 \\ 0 \\ 0 \\ 0 \\ 0 \\ 0 \\ 0 \end{bmatrix} + \Lambda^2 \begin{bmatrix} 0 \\ 1 \\ 1 \\ 1 \\ 0 \\ 0 \\ 0 \end{bmatrix} + \Lambda^3 \begin{bmatrix} 0 \\ 0 \\ 0 \\ 0 \\ 1 \\ 1 \\ 1 \end{bmatrix}$

The loading of the model consists of various combinations of independent configurations of gravity loads imposed at the free joints. Table 3.2 lists the different load combinations considered in this thesis and the corresponding figures presenting the stability boundaries. Tables 3.3 - 3.8 accompany Figs. 3.2 - 3.7 and define the points, and their characteristics, used to construct the stability boundaries. In Tables 3.3 - 3.7, points are numbered starting with the point on the vertical axis of the corresponding stability boundary and proceeding along the stability boundary to the horizontal axis point. In Figs. 3.2, 3.4 and 3.5, the large size of the point at the cusp indicates that the cusp location was not precisely determined. This imprecision is due to the use of the loading ray concept in the analysis process. In the discussion of this concept in Chapter 2, it is pointed out that the slope of the loading ray must be determined before starting the solution process. Unless the cusp occurs on a ray with symmetrical loading (see Fig. 3.3), the determination of the ray with the cusp is practically impossible.

In Tables 3.3 - 3.8, the column labeled "Joints Snapped Through" indicates those joints which exhibited snap-through at buckling. Snap-through is defined as a large increase in the displacement (in comparison with previous increases) in response to a small increase in the load. An easily

$$P = \Lambda^1 \begin{bmatrix} 1 \\ 0 \\ 0 \\ 0 \\ 0 \\ 0 \\ 0 \end{bmatrix} + \Lambda^2 \begin{bmatrix} 0 \\ 1 \\ 1 \\ 1 \\ 0 \\ 0 \\ 0 \end{bmatrix}$$

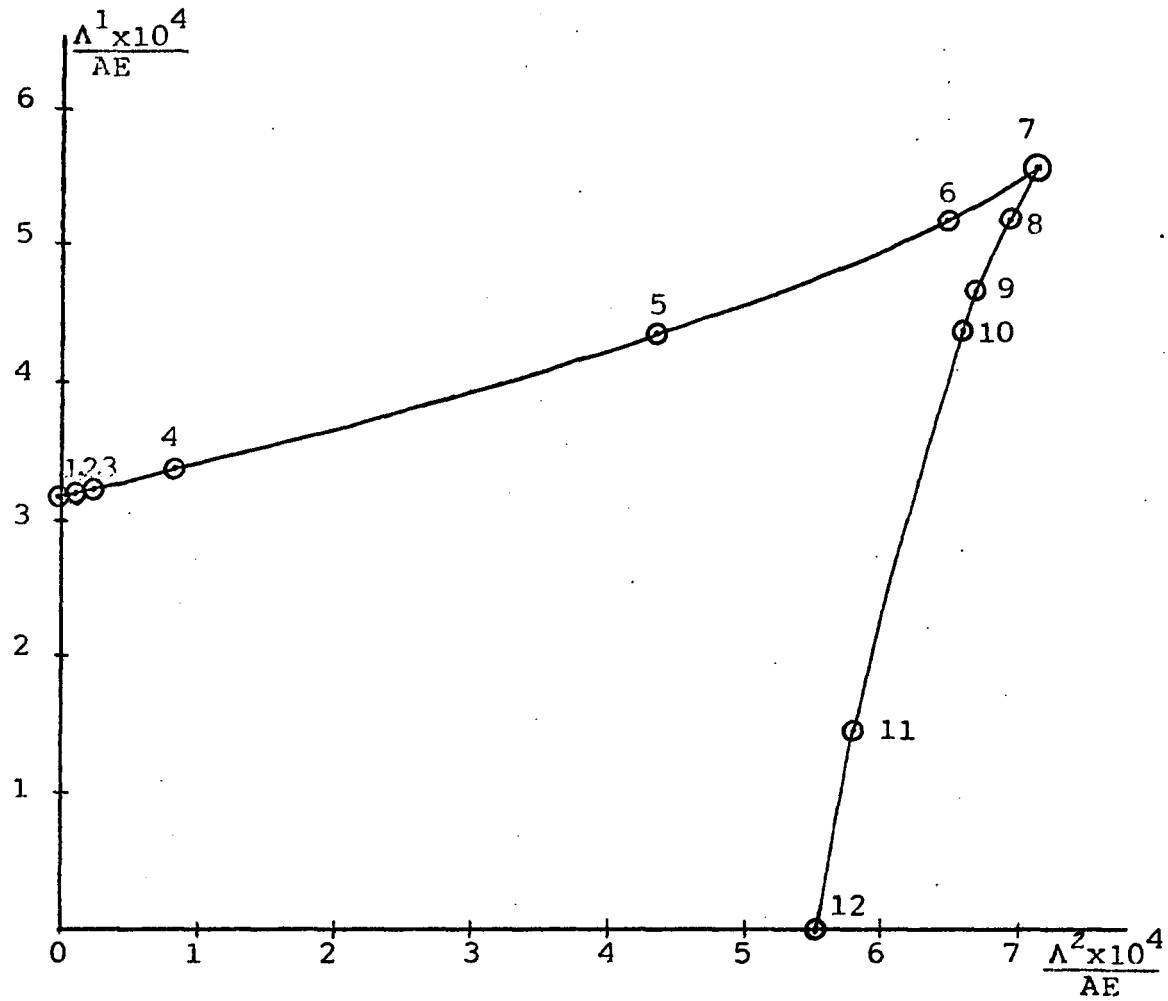

FIGURE 3.2 STABILITY BOUNDARY; LOAD COMBINATION A

TABLE 3.3

POINTS USED TO PLOT FIG. 3.2

PT	$\Lambda^1_{CR} \times 10^4$	$\Lambda^2_{CR} \times 10^4$	CLASSIFICATION	JOINTS SNAPPED THROUGH
1	3.156	0.000	Limit	1
2	3.188	0.128	Limit	1
3	3.216	0.257	Limit	1
4	3.355	0.838	Limit	1
5	4.334	4.334	Limit	1
6	5.160	6.450	Limit	1
7	5.528	7.088	Bifurcation?	1
8	5.175	6.900	Limit	4
9	4.655	6.650	Limit	4
10	4.371	6.556	Limit	2,4,6
11	1.442	5.769	Limit	2,4
12	0.000	5.513	Limit	2,4

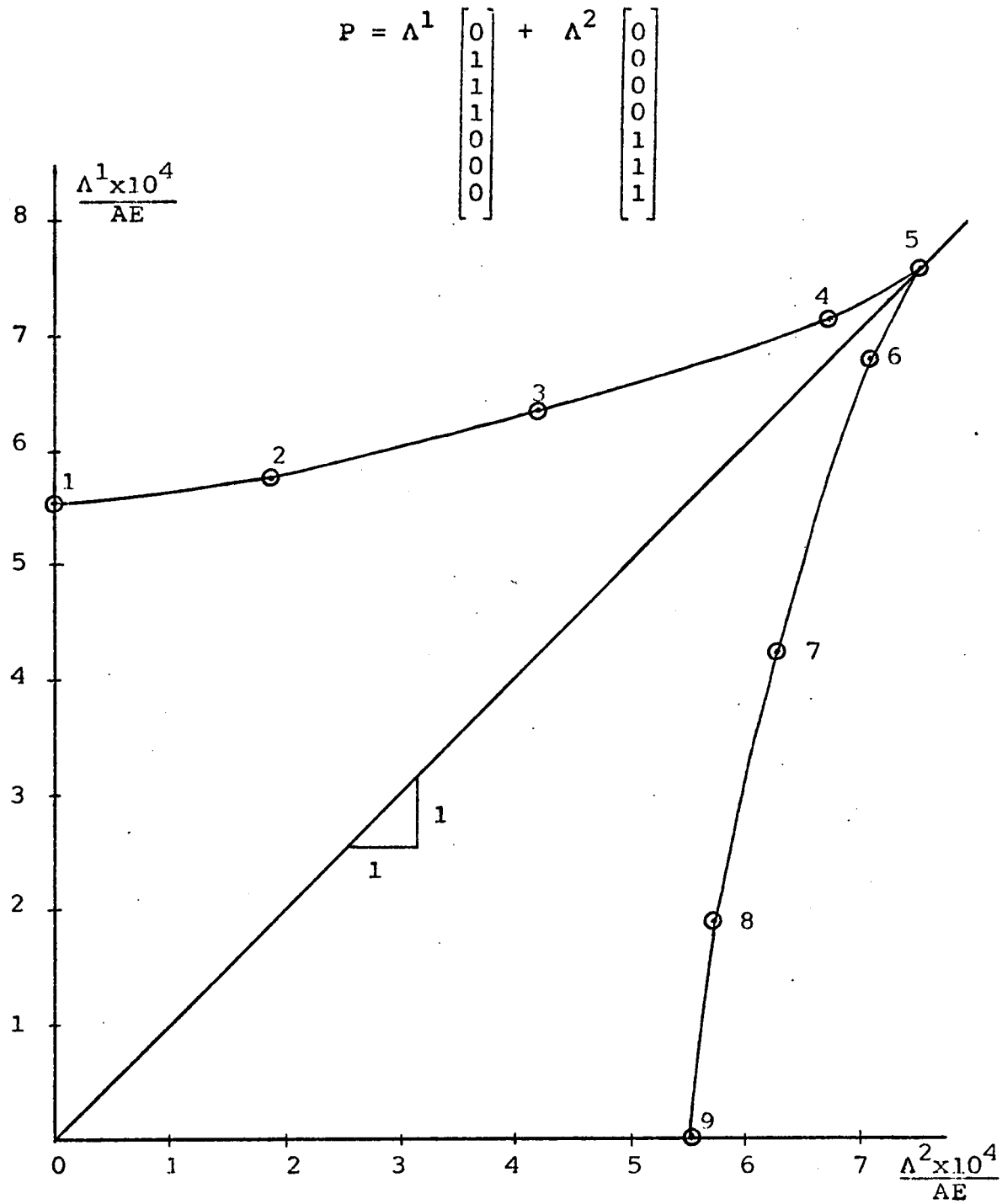

FIGURE 3.3 STABILITY BOUNDARY; LOAD COMBINATION B

TABLE 3.4

POINTS USED TO PLOT FIG. 3.3

PT	$\Lambda^1_{CR} \times 10^{-4}$	$\Lambda^2_{CR} \times 10^{-4}$	CLASSIFICATION	JOINTS SNAPPED THROUGH
1	5.513	0.000	Limit	2,4
2	5.700	1.900	Limit	2,4
3	6.300	4.200	Limit	2,4
4	7.100	6.200	Limit	4
5	7.500	7.500	Bifurcation	4,7
		By Symmetry		
6	6.745	7.100	Limit	7
7	4.200	6.300	Limit	5,7
8	1.900	5.700	Limit	5,7
9	0.000	5.513	Limit	5,7

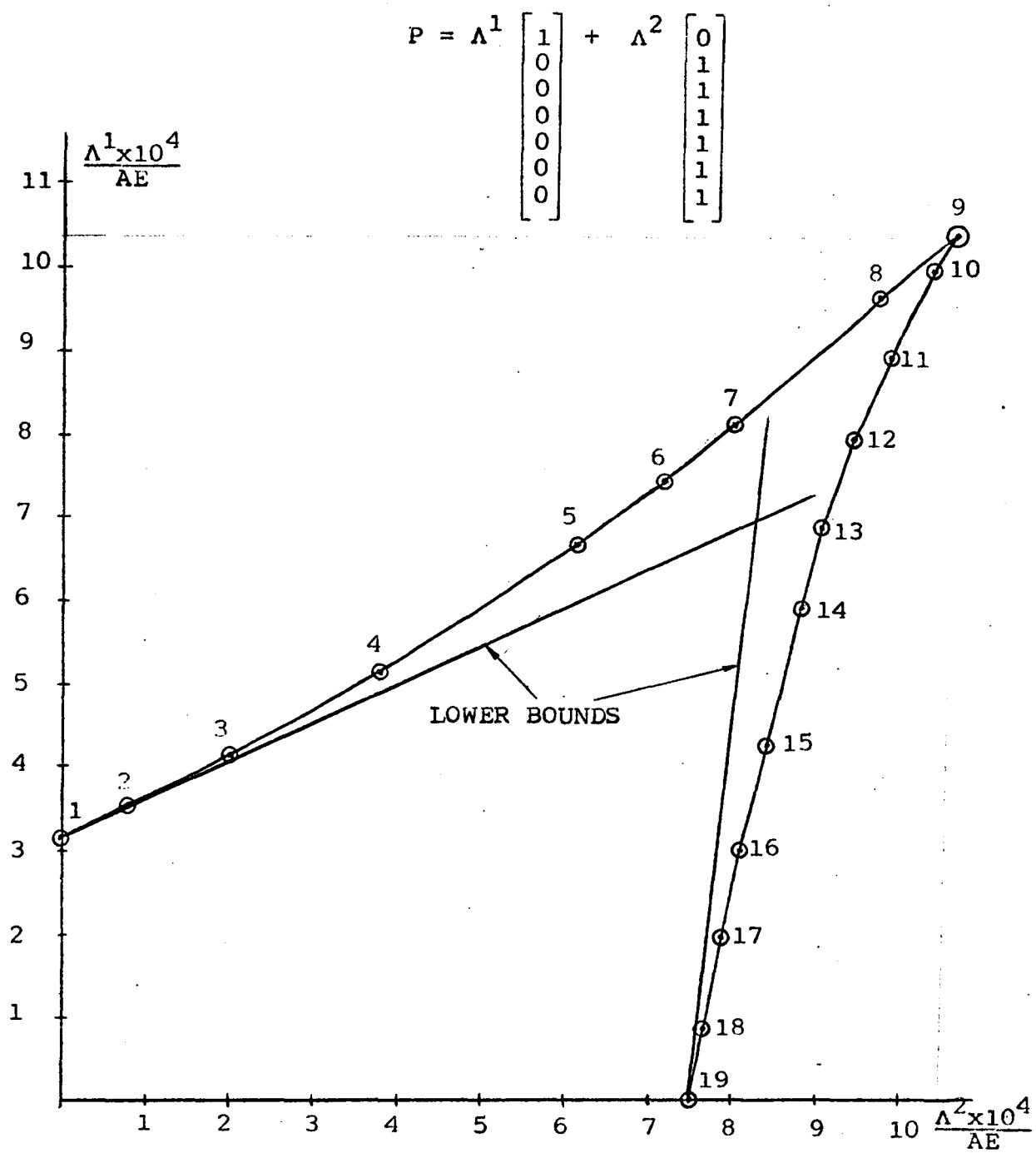

FIGURE 3.4 STABILITY BOUNDARY; LOAD COMBINATION C

TABLE 3.5

POINTS USED TO PLOT FIG. 3.4

PT	$\Lambda^1_{CR} \times 10^4$	$\Lambda^2_{CR} \times 10^4$	CLASSIFICATION	JOINTS SNAPPED THROUGH
1	3.156	0.000	Limit	1
2	3.572	0.893	Limit	1
3	4.169	2.084	Limit	1
4	5.163	3.872	Limit	1
5	6.647	6.182	Limit	1
6	7.399	7.219	Limit	1
✓7	8.031	8.031	Limit	1
8	9.557	9.796	Limit	1
✓9	10.274	10.654	Bifurcation?	Undetermined
10	9.909	10.405	Bifurcation?	All
11	8.910	9.900	Bifurcation	Undetermined
12	7.916	9.500	Bifurcation?	Undetermined
13	6.844	9.125	Bifurcation?	Undetermined
14	5.900	8.850	Bifurcation?	Undetermined
15	4.200	8.400	Bifurcation	3,6
16	3.038	8.100	Bifurcation?	2,4,6
17	1.975	7.900	Bifurcation?	3,5,7
18	0.963	7.700	Bifurcation?	4,6
19	0.000	7.500	Bifurcation	4,7

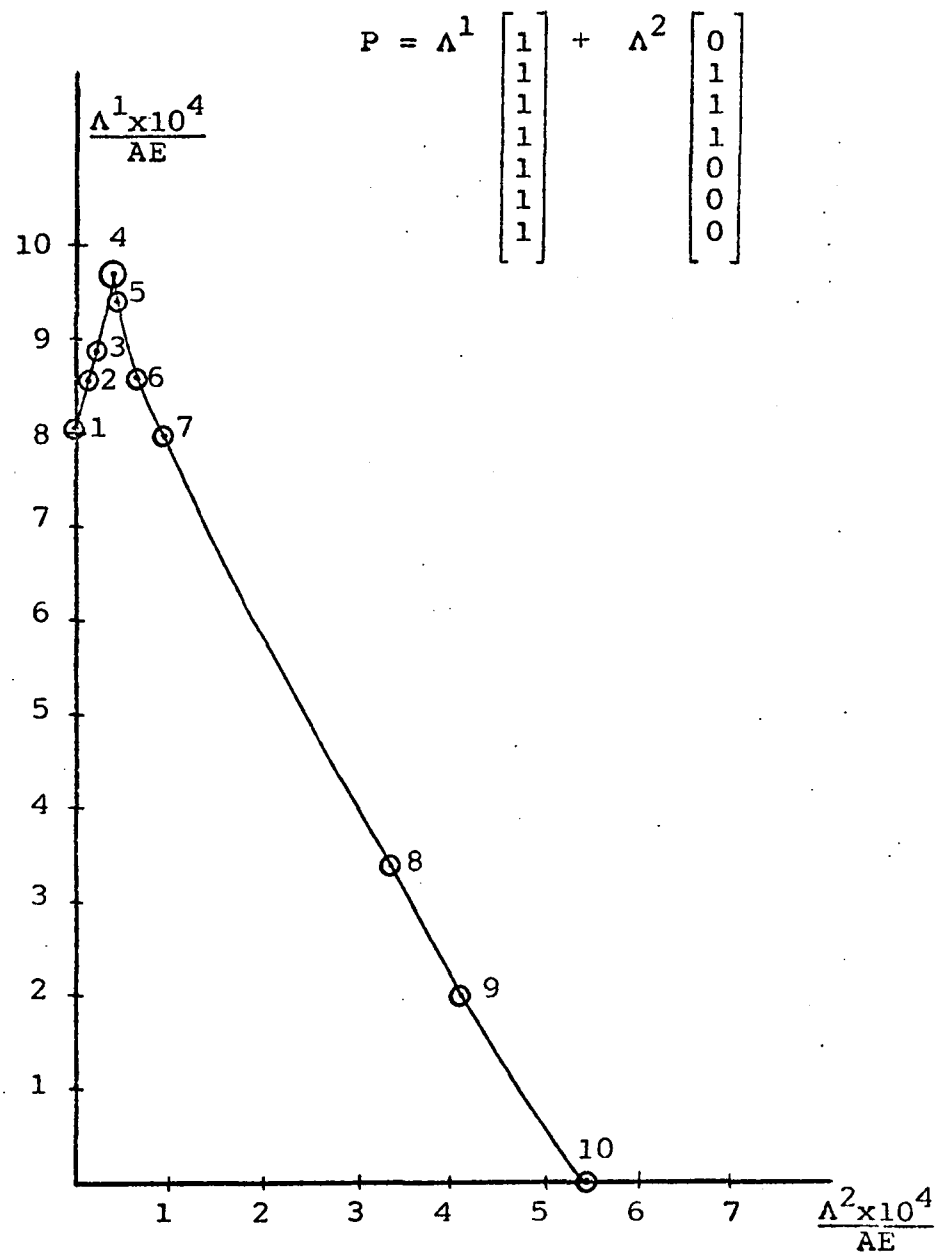

FIGURE 3.5 STABILITY BOUNDARY; LOAD COMBINATION D

TABLE 3.6

POINTS USED TO PLOT FIG. 3.5

PT	$A^1_{CR} \times 10^4$	$A^2_{CR} \times 10^4$	CLASSIFICATION	JOINTS SNAPPED THROUGH
1	8.031	0.0000	Limit	1
2	8.545	0.2136	Limit	1
3	8.868	0.3104	Limit	1
4	9.702	0.4370	Bifurcation?	All
5	9.433	0.4717	Limit	All
6	8.592	0.7160	Limit	All
7	8.011	1.0010	Limit	2,4
8	3.375	3.3750	Limit	2,4
9	2.050	4.1000	Limit	2,4
10	0.000	5.5130	Limit	2,4

$$P = \Lambda^1 \begin{bmatrix} 1 \\ 0 \\ 0 \\ 0 \\ 0 \\ 0 \\ 0 \end{bmatrix} + \Lambda^2 \begin{bmatrix} 1 \\ 1 \\ 1 \\ 1 \\ 1 \\ 1 \\ 1 \end{bmatrix}$$

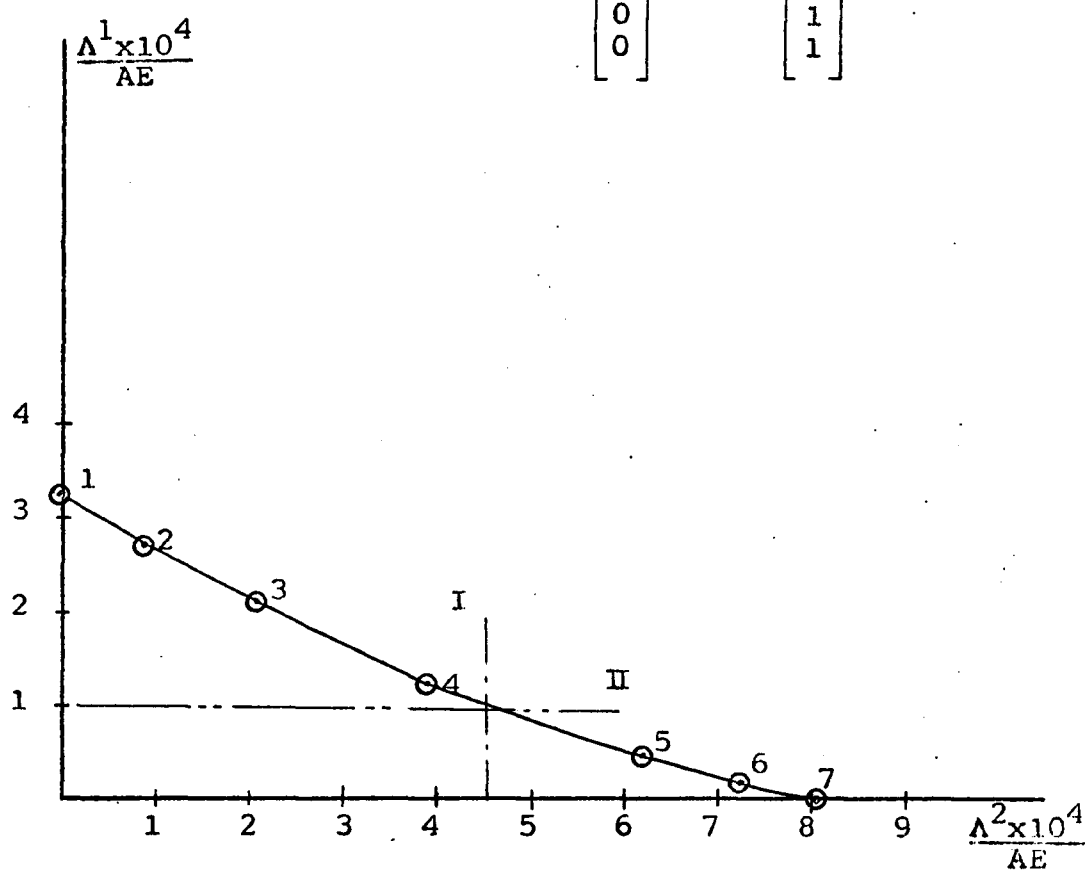

FIGURE 3.6 STABILITY BOUNDARY; LOAD COMBINATION E

TABLE 3.7

POINTS USED TO PLOT FIG. 3.6

PT	$\Lambda^1_{CR} \times 10^4$	$\Lambda^2_{CR} \times 10^4$	CLASSIFICATION	JOINTS SNAPPED THROUGH
1	3.156	0.000	Limit	1
2	2.679	0.893	Limit	1
3	2.084	2.084	Limit	1
4	1.291	3.872	Limit	1
5	0.465	6.182	Limit	1
6	0.181	7.219	Limit	1
7	0.000	8.031	Limit	1

$$P = \Lambda^1 \begin{bmatrix} 1 \\ 0 \\ 0 \\ 0 \\ 0 \\ 0 \\ 0 \end{bmatrix} + \Lambda^2 \begin{bmatrix} 0 \\ 1 \\ 1 \\ 1 \\ 0 \\ 0 \\ 0 \end{bmatrix} + \Lambda^3 \begin{bmatrix} 0 \\ 0 \\ 0 \\ 0 \\ 1 \\ 1 \\ 1 \end{bmatrix}$$

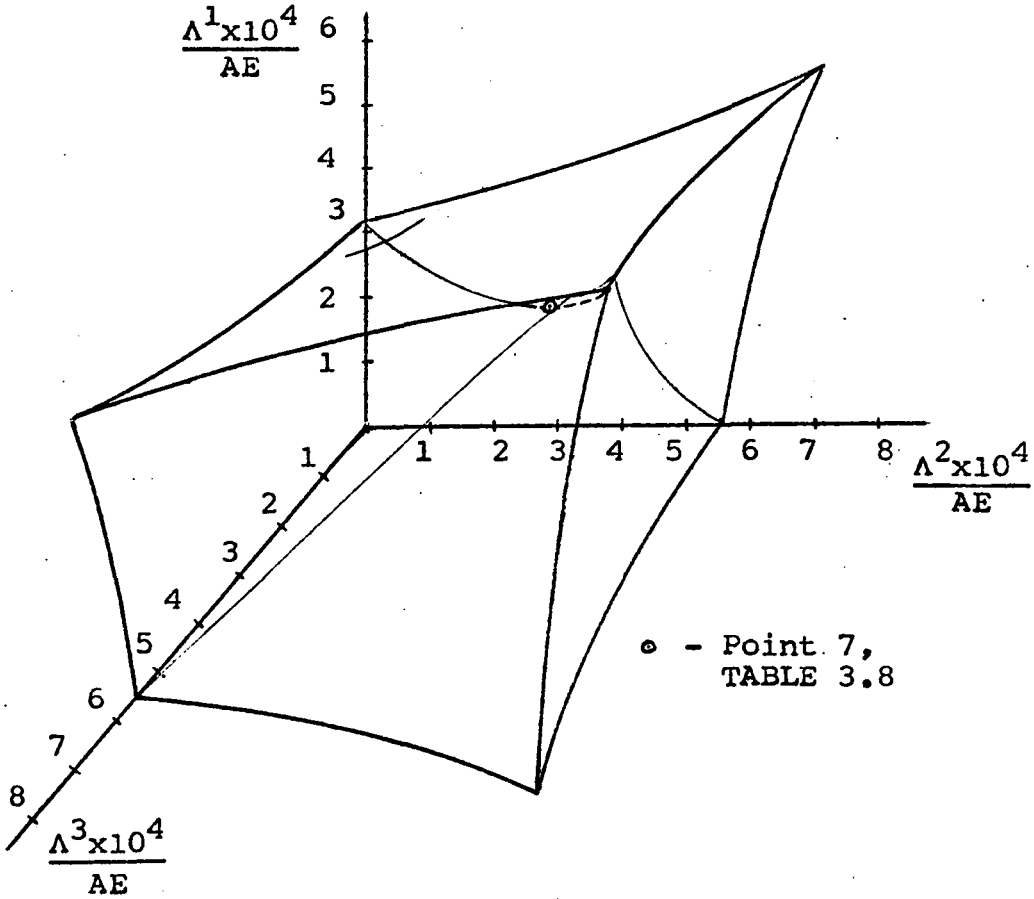

FIGURE 3.7 STABILITY BOUNDARY; LOAD COMBINATION F

TABLE 3.8

POINTS USED TO PLOT FIG. 3.7

PT	$\Lambda^1_{CR}\times10^4$	$\Lambda^2_{CR}\times10^4$	$\Lambda^3_{CR}\times10^4$	CLASSIFICATION	JOINTS SNAPPED THROUGH
			From FIGS. 3.4 and 3.6		
1	3.156	0.000	0.000	Limit	1
2	3.572	0.893	0.893	Limit	1
3	4.168	2.084	2.084	Limit	1
4	5.163	3.872	3.872	Limit	1
5	6.647	6.182	6.182	Limit	1
6	7.399	7.219	7.219	Limit	1
7	8.031	8.031	8.031	Limit	1
8	9.557	9.796	9.796	Limit	1
9	10.274	10.654	10.654	Bifurcation?	Undetermined
10	9.909	10.405	10.405	Bifurcation?	All
11	8.910	9.900	9.900	Bifurcation?	Undetermined
12	7.916	9.500	9.500	Bifurcation?	Undetermined
13	6.844	9.125	9.125	Bifurcation?	Undetermined
14	5.900	8.850	8.850	Bifurcation?	Undetermined
15	4.200	8.400	8.400	Bifurcation	3,6
16	3.038	8.100	8.100	Bifurcation?	2,4,6
17	1.975	7.900	7.900	Bifurcation?	3,5,7
18	0.963	7.700	7.700	Bifurcation?	4,6
19	0.000	7.500	7.500	Bifurcation	4,7
			From FIG. 3.2		
20	3.188	0.128	0.000	Limit	1
21	3.216	0.257	0.000	Limit	1
22	3.355	0.838	0.000	Limit	1
23	4.334	4.334	0.000	Limit	1
24	5.160	6.450	0.000	Limit	1
25	5.528	7.088	0.000	Bifurcation?	1
26	5.175	6.900	0.000	Limit	4
27	4.655	6.650	0.000	Limit	2,4,6
28	4.371	6.556	0.000	Limit	2,4,6
29	1.442	5.769	0.000	Limit	2,4

Points 1-19 lie in the plane of symmetry, points 20-43 lie on the half of the surface which contains the Λ^2 axis. Symmetry is used to construct the opposing half of the total surface.

TABLE 3.8 (CONTINUED)

PT	$\Lambda^1_{CR} \times 10^4$	$\Lambda^2_{CR} \times 10^4$	$\Lambda^3_{CR} \times 10^4$	CLASSIFICATION	JOINTS SNAPPED THROUGH
30	0.000	5.513	0.000	Limit	2,4
			From FIG. 3.3		
31	0.000	5.700	1.900	Limit	2,4
32	0.000	6.300	4.200	Limit	2,4
33	0.000	7.100	6.745	Limit	4
			From FIG. 3.5		
34	8.545	8.759	8.545	Limit	1
35	8.868	9.179	8.868	Limit	1
36	9.702	10.139	9.702	Bifurcation?	All
37	9.433	9.905	9.433	Limit	All
38	8.592	9.308	8.592	Limit	All
39	8.011	9.013	8.011	Limit	2,4
40	3.375	6.750	3.375	Limit	2,4
41	2.050	6.150	2.050	Limit	2,4
			Additional Points To Show Smoothness of "Uppermost" Surface		
42	3.572	1.072	0.714	Limit	1
43	3.575	1.251	0.536	Limit	1

Points 1-19 lie in the plane of symmetry, points 20-43 lie on the half of the surface which contains the Λ^2 axis. Symmetry is used to construct the opposing half of the total surface.

visualized example is Point 1 of Table 3.3; at the buckling load, joint 1 snapped approximately 4 units in the X-direction.

In the column labeled "Classification" in Tables 3.3 - 3.8, the type of failure is classified as a limit or bifurcation point. Some of the bifurcation point classifications are shown with question marks, for example, Point 7 of Table 3.3. The question mark indicates that classification is not proved, but is based on at least one of two hypothesized methods of classification. The behavior of the energy minimization program used in this study, which was previously discussed in this regard, provides one of these methods of classification. Another basis for classification is Huseyin's theory, which classifies the failure at a cusp in the stability boundary as a bifurcation point.

Fig. 3.7 presents a stability boundary surface describing the interaction of three independent load configurations. Upon close inspection this stability boundary can be seen to contain all the curves presented in Figs. 3.2 - 3.6; it was, in fact, constructed from these curves. The heavy lines contained within the load space, that is, excluding those lines contained in the planes defined by load axes, indicate ridges which are discontinuities in the slope of the surface. The thin lines show space curves traced on the surface. The three smooth surfaces appear to be composed of limit points, while the ridges appear to be composed of bifurcation points.

3.2 Discussion of Results

Although the stated purpose of this thesis goes beyond presenting a set of design aids for the studied structure, the use of stability boundaries as design aids is a very practical reason for their study. Two of the stability boundaries presented (Figs. 3.5 and 3.6) show the interaction of a uniformly distributed load configuration with other possible load configurations. These two stability boundaries can be used as design aids for this structure in the following manner. Fig. 3.6 is used to demonstrate the method. Construct a line representing the dead weight (uniform load) times the safety factor (line I, Fig 3.6). Now construct a line representing the maximum live load (such as a concentrated snow load at the apex) times the safety factor (line II, Fig. 3.6). If the rectangle formed is not wholly contained in the region of stability, as it is here, then the design should be reconsidered.

The stability boundary presented in Fig. 3.7 is not directly useful as a design aid because of the difficulty in locating a point on a three dimensional surface portrayed in two dimensions. However, it can provide an indication of the shape of a stability boundary for a uniformly distributed load configuration and any other independent load configuration formed by a combination of the load configurations at the axes. The method of deriving this boundary shape information is presented here in two steps.

The first step consists of visualizing the two loading rays defined by the uniformly distributed load configuration and the other load configuration in question. The loading ray for the uniformly distributed load configuration extends from the origin through a point defined by Point 7 of Table 3.8, which is marked on Fig. 3.7 for convenience. The second step is to visualize the intersection of the plane containing the two loading rays with the stability boundary surface. The portion of the curve defined by this intersection and lying between the two loading rays, indicates the general shape of the stability boundary which would result from the interaction of the two load configurations represented by the two loading rays.

The more a designer understands about stability boundaries, the more useful they will be to him as design aids. A detailed study of stability boundaries begins with a consideration of the points composing them. An inspection of Tables 3.3 - 3.8 indicates that the majority of failures are limit points. The implication is that under the majority of loading conditions, the structure will undergo significant nonlinear pre-buckling deformation. A comparison of the behavior of this reticulated dome with the behavior of shallow arches, which also exhibit nonlinear pre-buckling deformation, is interesting. The preponderance of limit point failures was noted in the arch studies of Plaut [27]

and Welton [39]. However, those studies indicated that bifurcation point failures occurred when symmetrical loads were imposed on symmetrical arches. This does not appear to be the case with the reticulated dome. Points 1 - 8 of Table 3.5 present symmetrical load configurations which resulted in limit points, and there is no apparent symmetry in the load configurations of Point 7 of Table 3.3 or Point 4 of Table 3.6, both of which are classified as bifurcation point failures.

The variety of buckled shapes which occur is indicated by the different joints which snapped-through under different load configurations. These different buckled shapes provide information which indirectly supports the classification of critical points at cusps as bifurcation points. Tables 3.3, 3.4, and 3.6 appear to indicate that independent load configurations which exhibit limit point failures resulting in different buckled shapes when acting alone will interact to form stability boundaries characterized by two smooth curves composed of limit points which meet at a cusp which is a bifurcation point. However, the classification of the cusp critical point is only proved for the cusp in Fig. 3.3 (corresponding to Table 3.4). To proved the classification of the cusp critical point in Figs. 3.2 and 3.5 (corresponding to Tables 3.3 and 3.6, respectively), these points would have to be located exactly. The difficulty of finding

the exact locating of these points has already been observed. Here, a hypothesis is presented which supports classification of these cusps as bifurcation points.

At the limit points on either side of the cusp one of the independent load configurations dominates the total load and thus determines the single buckling mode associated with a limit point. The buckled shapes at these limit points provide no information about the buckling mode itself, but do demonstrate which load configuration is dominant. Starting at a load axis and proceeding along the stability boundary toward the cusp, identical (Points 1 - 6, Table 3.3) or similar (Points 12 - 8, Table 3.3) buckled shapes indicate that the dominant load configuration along the curve of limit points does not change and is the load configuration at the axis. The minor changes in the buckled shapes which occur are due to the influence of the non-dominant load.

As the stability boundary passes through a cusp the changes in the buckled shapes indicate a change in the dominant load configuration. Therefore, at the cusp, the magnitudes of the two load configurations are somehow balanced so that neither is dominant. This in turn indicates that either of the two different buckling modes associated with the two different load configurations is possible. The existence of two different buckling modes for the same equilibrium state is characteristic of bifurcation. Therefore, the cusp must be a bifurcation point.

The bifurcation points in Figs. 3.2, 3.3, and 3.5 are all located at the cusps in these figures. However, Fig. 3.4 demonstrates the existence of a smooth curve composed entirely of bifurcation points. The construction of Fig. 3.7 demonstrated that this curve formed a ridge in the surface, but raised another question. All the bifurcation points in Table 3.8, with one exception, occur at ridges in the surface. The one exception is Point 9, Table 3.8 (this is the same point as Point 9, Table 3.5) which occurs at a three dimensional cusp. The question is, what characteristic of the point causes it to form a three dimensional cusp?

The hypothesis presented above supports the existence of two simultaneous buckling modes at a cusp in two dimensions which lies at the intersection of smooth curves composed of limit points. If this hypothesis is valid, then there is reason to believe that three simultaneous buckling modes exist at the cusp in three dimensions. The support for this conjecture is stated as follows. The three dimensional cusp lies at the intersection of three smooth surfaces composed of limit points. Logically, three separate buckling modes are associated with the three surfaces. If the hypothesis above is valid, at the intersection of the three surfaces the three separate buckling modes exist simultaneously.

The "peaking" of load magnitudes which occurs at cusps is another interesting feature of these points. Apparently a loading ray with a cusp defines a particular combination of the independent load configurations which results in an optimal distribution of stress among the members. This is not to imply that equal stresses exist in all the members at a cusp, but that the distribution of stress is more balanced at a cusp than not at a cusp. An example supporting this notion of balance is presented here.

Table 3.9 shows the stresses just prior to buckling in three typical members under two symmetric loadings, one of which forms a cusp. Type I members all meet at the apex, Type II members form the hexagonal "ring" around the apex, and Type III members lead to the supports, or fixed joints (see Fig. 3.1). Due to the load symmetry, the stress values presented are reasonably representative of stresses in members of each type. Note the relative similarity of the stresses in member Types I and II for Point 9, Fig. 3.4 (a cusp) as opposed to those same stresses for Point 1, Fig. 3.4. Also not that this has allowed the Type I members at Point 9 to be stressed to more than twice the value shown for Type I members at Point 1, Fig. 3.4. The "balance" in the stresses of Type I and II members at Point 9 is certainly why the magnitude of the apex load at Point 9, Fig. 3.4 is more than three times the magnitude of the apex load at Point 1, Fig. 3.4.

TABLE 3.9

STRESS DISTRIBUTION

MEMBER TYPE	JOINT INCIDENCE	$\frac{\sigma}{E}$ Just Prior to Buckling	
		POINT 1 Fig. 3.4	POINT 9 Fig. 3.4
I	1-2	-0.00109	-0.00223
II	2-3	+0.00093	-0.00199
III	2-8	-0.00013	-0.00362

- indicates compression

+ indicates tension

Returning to practical considerations of stability boundaries, perhaps their most important characteristic, to the designer, is their general shape. If the designer knows the general shape beforehand, he can determine new stability boundaries he needs using fewer points (and less analysis time) to locate these new boundaries. All the stability boundaries determined in this thesis are convex or piecewise convex toward the origin. It seems logical to assume that new stability boundaries for the studied structure would also be convex toward the origin.

Prediction of stability boundary shape for reticulated structures other than the dome studied here is difficult. It is not reasonable, based only on the results presented here, to make assuptions about convexity of boundaries for reticulated structures in general. The observations leading to the hypothesis concerning bifurcation at cusps may provide a basis for assuming the existence of at least one cusp somewhere in a load plane defined by independent load configurations which exhibit different buckled shapes when acting alone. Additionally, the idea of a certain combination of independent load configurations causing an optimal stress distribution, which was used to explain the peaking of load values of a cusp, makes the existence of many cusps in one plane seem unreasonable. However, there may be some reticulated geometry for which these ideas do not apply.

There appears to be only one published stability boundary for a reticulated structure other than the structure studied here, so the validity of the notions concerning boundary shape cannot be checked. If stability boundaries are to be used as design aids, they will have to be determined individually for the structure under consideration.

The exact determination of a stability boundary takes time even when its general shape is known, and the designer may require many stability boundaries for a structure. To concerve analysis time, a method of estimating lower bounds [1] is reviewed here. The designer must first ascertain, by developing a reasonable number of stability boundaries, whether the boundaries are convex or concave toward the origin. The development of a stability boundary surface may be helpful in this regard.

If the stability boundaries are consistently concave toward the origin, the designer need only determine the critical magnitudes of each independent load configuration acting alone. The lower bound is formed by a straight line joining these two load axis points (see Fig. 3.8). If the stability boundaries are consistently convex toward the origin, the designer must determine small sections of the stability boundary in the vicinity of the two load axes. The lower bound is formed by constructing tangents to the stability boundary at the load axes (see Fig. 3.4).

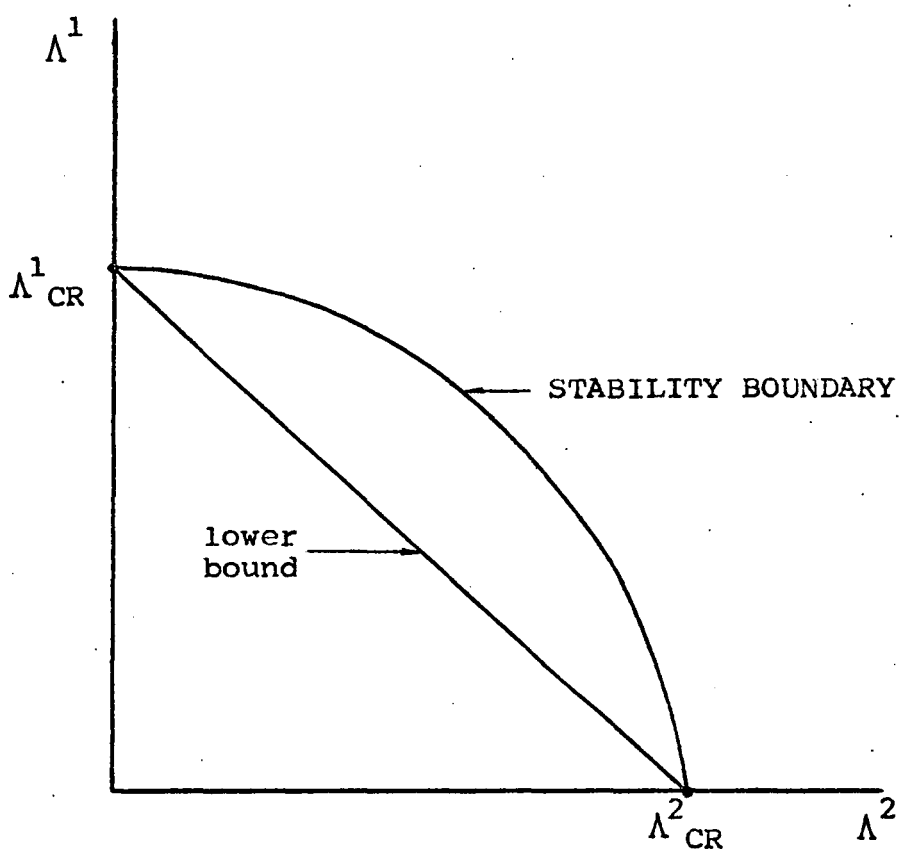

FIGURE 3.8 CONCAVE STABILITY BOUNDARY

3.3 The Theory of Huseyin

The previous discussion of lower bounds demonstrates the value of knowing whether a stability boundary is conve or concave toward the origin. Therefore the following theorem, presented by Huseyin, is of interest since it implies that convexity or concavity can be determined without constructing the entire stability boundary. This theorem is stated as follows.

> If the general critical point is elliptic, then, the associated stability boundary cannot have convexity toward the origin. In the case of two parameters, a necessary and sufficient condition for convexity toward the origin is the possiblity of bifurcation at the critical point [14].

To fully understand this theorem, a number of terms must be explained. In the general theory of Huseyin, critical points are classified as general critical points and special critical points. The theorem above applies only to general critical points, which are subclassified as elliptic, hyperbolic, and singular.

Huseyin's classification system is mathematical and makes use of his method of solution, which is a diagonalized perturbation scheme. At a critical point, the vanishing of certain terms in the expanded equilibrium equations determines the classification of the point [14]. The static perturbation program used in this study would have required extensive rewriting to make use of Huseyin's mathematical

criteria, since the necessary terms were not computed and diagonalization was specifically avoided [1]. Moreover, the perturbation program became numerically unstable at many bifurcation points.

An attempted classification of critical points which did not rely on Huseyin's solution method failed because of the lack of generally applicable classification criteria. At present, the application of Huseyin's convexity theorem appears restricted to those problems solved by Huseyin's solution method.

CHAPTER 4

CONCLUSIONS

The stability of a reticulated dome with 21 degrees of freedom under multiple independent static loads is investigated. The model considered is elastic and geometrically nonlinear, and assumes that the joints have no moment resisting capacity.

Two computer programs based on different numerical analysis techniques are used to determine the nonlinear response of the model to the loads. The functioning of the programs is briefly discussed and a comparison of the two is made. The program based on the principle of minimum potential energy was found to be more reliable and easier to formulate. The program based on the static perturbation technique was found to be more efficient and could be made to supply reliable information necessary for the classification of critical points as bifurcation points. The accuracy of the two programs is verified by a comparison of program solutions with an exact solution for a problem with a closed form solution. Due to its reliability, the energy minimization program was used to determine all solutions. The static perturbation program was occasionally used to check solutions for validity and to prove the classification of a critical point.

The solution results are presented in the form of stability boundaries, which depict the interaction of

independent loads. Five stability boundaries for various pairs of independent load configurations and one stability boundary for three independent load configurations are presented. The use of these stability boundaries as design aids to show variance in the safety factor is discussed.

The relationship of the classification of a critical point to the smoothness of the stability boundary at that point is discussed. Limit points consistently form smooth boundaries. Bifurcation points may form either smooth curves or cusps (points with discontinuous slope) on two dimensional stability boundaries. Bifurcation points on three dimensional stability boundaries are consistently located at points where the slope of the surface is not continuous in all directions.

A hypothesis supporting the classification of some cusps as bifurcation points is presented. Application of this hypothesis does not require the exact location of the cusp. The hypothesis is based on the intuitive observation that a gradual transformation of one distinct buckling mode into another distinct buckling mode does not occur. This intuitive observation may possibly be used to predict cusp formation in stability boundaries for other reticulated structures.

An explanation is given for the occurrence of maximum load values at cusps. The basis of this explanation is the conjecture that the combination of loads at the cusp

represents an optimal load combination which results in a greater degree of balance in the distribution of stress among the individual members of the structures. A simple presentation showing the distribution of stress at a cusp versus the distribution of stress at another point on the same stability boundary provides support for the notion of an optimal combination of loads at a cusp. The association of a cusp with an optimal load combination for this structure implies that, for any structure, the number of cusps in a stability boundary will be equivalent to the number of independent load combinations which result in the most efficient stress distributions.

The difficulty of predicting the general shape of a stability boundary for an arbitrary structure is discussed. Part of this difficulty is due to the lack of published stability boundaries, since other published stability boundaries could be used to check the general validity of observations and ideas concerning boundary shape which were drawn from this study. An efficient method of determining lower bounds to arbitrary stability boundaries is reviewed; however, this method requires knowledge of the general shape of the stability boundary.

A theorem due to Huseyin concerning convexity of stability boundaries is reviewed. The theorem is found to depend on a system of critical point classification which is not universally applicable. This dependence seriously

limits the applicability of the theorem and prevented its application to the problem studied here.

The lack of published stability boundaries for reticulated structures in general limited the number of useful observations which could be drawn from this study, and confined the application of these observations to the structure which was studied. Comparison of stability boundaries for different reticulated structures might make it possible to associate certain general boundary shapes with certain structures. Such comparison would also allow the validity of some of the ideas presented here to be tested. The development of stability boundaries for a number of different reticulated structures is recommended for future study.

BIBLIOGRAPHY

1 Abatan, A. O., Stability of Reticulated Domes Under Multiple Static and Dynamic Loads, Ph.D. Dissertation, Virginia Polytechnic Institute & State University, Blacksburg, Virginia, 1976.

2 Abatan, A. O. and Holzer, S. M., "Degree of Stability of Geodesic Domes with Independent Loading Parameters," Journal of Computers and Structures, CAS 545 (L), 1977, pp. 1-9.

3 Aguilar, R. J., "Snap Through Buckling of Framed Triangulated Domes", Journal of the Structural Division, ASCE, Vol. 93, No. ST2, 1967, pp. 301-317.

4 Crooker, J. O. and Buchert, K. P., "Reticulated Space Structures," Journal of the Structural Division, ASCE, Vol. 96, No. ST3, Mar. 1970, pp. 687-700.

5 Dadeppo, D. A. and Schmidt, R., "Large Deflections and Stability of Hingeless Circular Arches Under Interacting Loads," Journal of Applied Mechanics, ASME, Vol. 41, Series E, No. 4, Dec. 1974, pp. 989-994.

6 Dadeppo, D. A. and Schmidt, R., "Stability of an Arch Under Combined Loads, Bibliography on Stability of Arches," Journal of Industrial Mathematics Society, Vol. 20, Part 2, 1970, pp. 71-89.

7 Dadeppo, D. A. and Schmidt, R.," Stability of Two Hinged Circular Arches with Independent Loading Parameters," AIAA Journal, Vol. 12, No. 1-6, Mar. 1974, pp. 385-386.

8 Dean, D. L. and Ugarte, C. P., "Discussion on Membrane Forces and Buckling in Reticulated Shells by D. T. Wright (Feb. 1965)," Journal of the Structural Division, ASCE, Vol. 91, No. ST5, 1965, pp. 378-385.

9 Ekstrom, R. E., "Buckling of Cylindrical Shells Under Combined Torsion and Hydrostatic Pressure, "Experimental Mechanics, Vol. 3, Aug. 1963, pp. 192-197.

10 Fletcher, R. and Powell, M. J. D., "A Rapidly Convergent Descent Method for Minimization," Computer Journal, Vol. 6, NO. 2, 1963, pp. 163-168.

11 Hangai, Y. and Kawamata, S., "Nonlinear Analysis of Space Frames and Snap-Through Buckling of Reticulated Shell Structures," IASS Pacific Symposium, Part II on Tension Structures and Space Frames, Tokyo and Kyoto, Oct. 1971.

12 Hangai, Y. and Kawamata, S., "Perturbation Method in the Analysis of Geometrically Nonlinear and Stability Problems," Advances in Computational Methods in Structural Mechanics and Design, J. J. Oden, et.al., (Editors), University of Alabama Press, Huntsville, Alabama, 1972, pp. 473-489.

13 Holzer, S. M., Somers, A. E. and White, W. S., "Stability of Lattice Structures Under Combined Loading," ASCE Fall Convention and Exhibit, Preprint No. 2975, San Francisco, Oct. 1977.

14 Huseyin, K., Nonlinear Theory of Elastic Stability, Noordhoff International Publishing, Leyden, The Netherlands, 1975.

15 Jagannathan, D. S., Epstein, H. I. and Christiano, P. P., "Snap-Through Buckling of Reticulated Shells," Proc. Institution of Civil Engineers, Part 2, 59, Dec. 1975, pp. 727-742.

16 Kadar, I., "Aluminum Space Structures in Hungary," ASCE National Structural Engineering Meeting, Preprint No. 1370, Baltimore, Maryland, April 1971.

17 Kahn, L. (Editor), Domebook 2, Shelter Publications, Bolinas, California, 1974

18 Langhaar, H. L., Energy Methods in Applied Mechanics, John Wiley and Sons, New York, 1962.

19 Loo, T. C. and Evan-Iwanowski, R. M., "Interaction of Critical Pressures and Critical Concentrated Loads Acting on Shallow Spherical Shells," Journal of Applied Mechanics, ASME, Vol. 33, No. 3, 1966, pp. 612-616.

20 Mahabaliraja and Durvasula, S., "Interaction Surfaces for Buckling under Combined Loading of Simply Supported Skew Plates," Proc. 15th Congress of Theoretical and Applied Mechanics, Indian Society of Theoretical and Applied Mechanics, 1970, pp. 115-136.

21 Makowski, Z. S., Steel Space Structures, Michael Joseph LTD., London, 1965.

22 Mandadi, V., On the General Theory of Stability and Its Applications, Ph.D. Thesis, University of Waterloo, Ontario, Canada, Sept. 1976.

23 Matthiesen, R. B. and MacCalden, P. B., "Combination Torsion and Axial Compression Tests of Conical Shells," AIAA Journal, Vol. 5, Feb. 1967, pp. 305-309.

24 Meirovitch, L., Methods of Analytical Dynamics, McGraw-Hill, New York, 1970.

25 Myachenkov, V. I., "Stability of Spherical Shells Under Combined Action of an External Pressure and Local Axisymmetric Loads," Akademiya Nauk SSSR, Nov.-Dec. 1970, pp. 133-138, translated 14 Nov. 1973, NISC.

26 Neale, K. W. and Lind, N. C., "Limit Analysis of Plates Under Combined Loads", Journal of the Engineering Mechanics Division, ASCE, Vol. 96, EM5, Oct. 1970, pp. 711-728.

27 Plaut, R. H., "Snap-through Instability of Shallow Arches Subjected to Multiple Concentrated Loads," Technical Report VPI-E-77-21, VPI & SU, Blacksburg, Virginia, Aug. 1977.

28 Renton, J. D., "Buckling of Frames Composed of Thin Walled Members, " Thin Walled Structures, A. H. Chilver (Editor), John Wiley and Sons, New York, 1967, pp. 1-59.

29 Richter, D. L., "Design of Geodesic Dome South Pole", ASCE Fall Convention and Exhibit, Preprint No. 3060, San Francisco, Oct. 1977.

30 Roorda, J., "Concepts in Elastic Structural Stability", Mechanics Today, S. Nemat-Nasser (Editor), Vol. 1, Pergamon Press 1974, pp. 322-370.

31 Sabir, A. B., "Large Deflection and Buckling Behavior of a Spherical Shell with Inward Point Load and Uniform External Pressure," Journal of Mechanical Engineering Science, Vol. 6, No. 4, 1964, pp. 394-404.

32 Sherbourne, A. M. and Haydl, H. M., "Plastic Analysis of Shallow Spherical Shells Under Combined Loading", ZAMM, Band 54, No. 2, Feb. 1974, pp. 73-82.

33 Sherbourne, A. M. and Haydl, A. M., "Limit Loads of Circular Plates Under Combined Loading," Journal of Applied Mechanics, ASME, Vol. 40, Sept. 1973, pp. 799-802.

34 Sherman, D. R., Chairman, "Lattice Structures: State of the Art Report," by the Task Committee on Latticed Structures of the Committee on Special Structures of the Committee on Metals of the Structural Division," Journal of the Structural Division, ASCE, Vol. 102, No. ST11, Nov. 1976, pp. 2197-2230.

35 Singer, J., "On Experimental Technique for Interaction Curves of Buckling of Shells," Experimental Mechanics, Vol. 4, Sept. 1964, pp. 279-280.

36 Thompson, J. M. T. and Hunt, G. W., A General Theory of Elastic Stability, John Wiley and Sons, London, 1973.

37 Timoshenko, S. P., Theory of Elastic Stability, McGraw-Hill, New York, 1936.

38 Weingarten, V. I. and Seide, P., "Elastic Stability of Thin-Walled Cylindrical and Conical Shells Under Combined External Pressure and Axial Compression, AIAA Journal, Vol. 3, May 1965, pp. 913-920.

39 Welton, R. H. B. III, Stability Analysis of Arch Models Under Multiple Loads, M. S. Thesis, Virginia Polytechnic Institute and State University, Blacksburg, Virginia, May, 1977.

40 Wongkoltoot, K., Degree of Stability of a Shallow Space Truss, Ph.D. Dissertation, Virginia Polytechnic Institute and State University, Blacksburg, Virginia, 1975.

41 Wright, D. T., "Instability in Reticulated Spheroids; Experimental Results and the Effect of Nodal Imperfections," Structures Technology for Large Radio and Radar Telescope Systems, Mar and Liebowitz (Editors) MIT Press, 1969, pp. 369-379.

42 Zarghamee, M. S. and Shah, J. M., "Stability of Space Frames," Journal of the Engineering Mechanics Division, ASCE, Vol. 94, No. EM2, Apr. 1968, pp. 371-383.

The vita has been removed from the scanned document

STABILITY OF A RETICULATED DOME UNDER MULTIPLE INDEPENDENT LOADS

by

Willis S. White, III

(ABSTRACT)

The primary purpose of this thesis is to investigate stability boundaries, or load interaction curves, of a reticulated dome. An elastic, geometrically nonlinear model with 21 degrees of freedom is considered.

The nonlinear response of the model to imposed loads is determined using two separate computer programs as a check on each other. One program is based on the static perturbation technique and the other is based on an energy minimization technique. Program solutions are compared with each other and with other published solutions. Various characteristics of the two programs are discussed.

Five stability boundaries for two independent loads and one for three independent loads are presented. These stability boundaries are all found to exhibit convexity or piecewise convexity toward the origin. Characteristics of points composing the stability boundaries are noted and discussed with emphasis placed on ways that point characteristics affect boundary shape. Three observations are noted:

1. Critical points classified as limit points

consistently form smooth boundaries, those classified as bifurcation points do not.

2. It is possible to predict the occurrence of a cusp in the stability boundary in certain load planes.

3. The occurrence of load maxima at cusps in stability boundaries is due to the higher degree of balance achieved in the stress distribution throughout the structure at that critical point.

In addition, a method of estimating lower bounds and a theorem dealing with convexity of stability boundaries are briefly discussed.